FEDERAL UNIVERSITY OF ITAJUBÁ
MECHANICAL ENGINEERING INSTITUTE

Damage Analysis in Mechanical Structures Using Vibrothermography

Lucas Antonio de Oliveira

Itajubá - MG/MG
2024

FEDERAL UNIVERSITY OF ITAJUBÁ
MECHANICAL ENGINEERING INSTITUTE

Damage Analysis in Mechanical Structures Using Vibrothermography.

Lucas Antonio de Oliveira

A dissertation presented to the Postgraduate Program of Mechanical Engineering, from the Mechanical Engineering Institute of the Federal University of Itajubá, as a requirement to obtain the title of Doctor of Science in Mechanical Engineering.

Concentration Area: Design, Materials, and Processes

Orientador: Prof. Dr. Sebastião Simões da Cunha Jr
Coorientador: Prof. Dr. Guilherme Ferreira Gomes

Itajubá - MG
2024

FEDERAL UNIVERSITY OF ITAJUBÁ
MECHANICAL ENGINEERING INSTITUTE

Damage Analysis in Mechanical Structures Using Vibrothermography.

A dissertation presented to the Postgraduate Program of Mechanical Engineering, from the Mechanical Engineering Institute of the Federal University of Itajubá, as a requirement to obtain the title of Doctor of Science in Mechanical Engineering.

Examination Board:

Prof. Dr. Marcelo Braga dos Santos (UFU)
Prof. Dr. Edson Hideki Koroishi (UTFPR)
Prof. Dr. Yohan Ali Diaz Mendez (IEM - UNIFEI)
Prof. Dr. Bruno Silva de Sousa (IEM - UNIFEI)
Prof. Dr. Guilherme Ferreira Gomes (IEM - UNIFEI)
Prof. Dr. Sebastião Simões da Cunha Júnior (IEM - UNIFEI)

Itajubá - MG
2024

"Success is the sum of small efforts repeated day after day."
(Robert Collier)

ACKNOWLEDGEMENTS

I thank my parents Antonio and Nildes, my fiancée Bárbara, and my brother Leandro for their unrestricted and unparalleled support.

To my advisors, Profs. Drs. Sebastião Simões da Cunha Júnior and Guilherme Ferreira Gomes, for all their guidance, correction, and shared knowledge. Without forgetting to thank my friends and colleagues in the GEMEC, ALLOY, NTC and LabTC groups for all their help during this stage of my life.

To the professors from inside and outside UNIFEI who took part in my qualification but were unable to attend the final stage.

In addition to the technicians from the vibration and composites laboratories and the UNIFEI team, we must also thank CAPES for its financial support, which was fundamental to carrying out this research.

ABSTRACT

This work aims to contribute to the development, understanding, and advancement of damage detection in composite materials using the technique of vibrothermography. This technique, classified as an active infrared thermography technique, uses vibrations to add energy to the system and thermal mapping of the material's surface to identify temperature profiles or gradients that indicate the possibility of internal damage to the structure. In the search for innovation in numerical analysis applied to the subject, the formulation proposed to evaluate the viscoelastic response of the material was applied, making it possible to detect the damage induced at the interface between the Prepreg and Rohacell Hero 71®materials. The change in the temperature profile generated on the surface of the material after numerical analysis of the structure made it possible to detect points with greater temperature gradients, such as the crimping region, the force application region and the region where the damage was inserted. In addition to the initial numerical analysis carried out for sinusoidal excitation, experimental tests were carried out to evaluate the generation of internal heat in the structure during excitation. At this stage, the use of different frequencies (natural and unnatural) and different types of signals (composed of sine, triangular or square waves) proposed to investigate the presence of damage in the sandwich beam were evaluated, obtaining different responses for the combinations used. A higher rate of internal heat generation was observed for excitation using the square type signal and lower for triangular type excitation. The measurement of the accelerations at the reference points defined in the test plan, together with the analysis of the thermograms generated for the different combinations, made it possible to verify, for the damage region, greater heat exchange between the beam and the environment when excited at a frequency of 545.65 Hz. At 938.96 Hz, for the damaged region, the lower energy exchange between the beam and the environment and the greater generation of internal heat when compared to the same undamaged region led to a change in the temperature profile, indicating the possibility of damage.

Key-words: infrared thermography, vibrothermography, non-destructive testing, viscoelasticity.

RESUMO

Este trabalho tem como objetivo contribuir com o desenvolvimento, entendimento e avanço da detecção de danos em materiais compósitos utilizando a técnica da vibrotermografia. Esta técnica classificada como uma técnica de termografia infravermelha ativa, utiliza de vibrações para adicionar energia ao sistema e do mapeamento térmico da superfície do material para identificar perfis ou gradientes de temperatura que indiquem a possibilidade da existência ou não de danos internos à estrutura. Na busca pela inovação nas análises numéricas aplicadas ao tema, a formulação proposta para avaliar a resposta viscoelástica do material foi aplicada, e permitiu realizar a detecção do dano induzido na interface entre os materiais Prepreg e Rohacell Hero 71®. A mudança no perfil de temperatura gerado na superfície do material após análise numérica da estrutura, permitiu detectar pontos com maiores gradientes de temperatura, como na região de engaste, na região de aplicação da força e a na região onde o dano foi inserido. Além da analise numérica inicial realizada para excitação do tipo senoidal, testes experimentais foram realizados para avaliar a geração de calor interno na estrutura durante a excitação. Nesta etapa, a utilização de diferentes frequências (naturais e não naturais) e de diferentes tipos de sinais (compostos por ondas senoidal, triangular ou quadrada) propostos para investigar a presença de danos na viga sanduiche foram avaliadas, obtendo-se diferentes respostas para as combinações utilizadas. Observou-se uma maior taxa de geração interna de calor para a excitação utilizando sinal do tipo quadrado e menor para a excitação do tipo triangular. A medição das acelerações nos pontos de referência definidos no planejamento dos ensaios, em conjunto com a análise dos termogramas gerados para as diferentes combinações, permitiu verificar para a região do dano, maiores trocas de calor entre a viga e o ambiente quando excitado na frequência de 545.65 Hz. Já para a frequência de 938.96 Hz, para a região do dano, a menor troca de energia entre a viga e o ambiente e a maior geração de calor interno quando comparada com a mesma região não danificada, permitiu observar uma mudança no perfil de temperatura, indicativo da possibilidade de existência de um dano.

Palavras-chaves: Termografia infravermelha, vibrothermogafia, ensaios não destrutivos, viscoelasticidade.

CONTENTS

LIST OF FIGURES

LIST OF TABLES

LIST OF ABBREVIATIONS AND ACRONYMS

BVID	Barely Visible Impact Damage	5
CFRP	Carbon Fiber Reinforced Polymer	5
CNTT	Carbon Nanotubes-Based Thermography	15
DMA	Dynamic Mechanical Analysis	27
DMT	Direct Material-Based Thermography	15
ECST	Eddy Current Stimulated Thermography	15
ERCM	Eletrical Resistance C. M. Coupled to Thermography	15
FBH	Flat Bottomed Hole	6
FMT	Frequency Modulated Thermography	15
FRF	Function Response Frequency	28
FT	Fourier Transform	16
GFRP	Glass Fiber Reinforced Polymer	5
ICA	Independent Component Analysis	15
IMT	Indirect Material-Based Thermography	15
IRT	Infrared Thermography	1
LDR	Local Defect Resonance	7
LIT	Lock-in Thermography	15
LLT	Laser-Line Thermography	15
LPT	Long Pulse Thermography	15
LST	Laser-Spot Thermography	15
MT	Metal-Based Thermography	15
MWT	Microwave Thermography	15
NUST	Nonlinear Ultrasonic Stimulated Thermography	15
OMA	Operational Modal Analysis	16
PCA	Principal Component Analysis	15
PCM	Polymer Matrix Composite	5
PCT	Principal Component Thermography	16
PPT	Pulsed Phase Thermography	16
PSD	Power Spectral Density	16
PT	Pulsed Thermography	15
SHT	Step-Heating Thermography	15
SHVT	Self-Heating Vibrothermography-Based	7
SMArt	Shape Memory Alloys-Based Thermography	15

LIST OF ABBREVIATIONS AND ACRONYMS

UST	Ultrasonic Stimulated Thermography	15

LIST OF SYMBOLS

E''	Loss modulus [Pa]	27
δ	Lag phase [°]	26
ω	Frequency [Hz]	26
ρ	Density [kg/m^3]	8
σ^2_{max}	Stress [Pa]	27
υ	Poisson's ratio [-]	8
f_{LDR}	Natural frequency of the defect [Hz]	8
k_{eff}	Stiffness effective [N/m]	8
A	Range [m]	26
D	Bending stiffness [N·m/rad]	8
d	Residual wall thickness of the FBH [m]	8
m	Mass of the FBH [kg]	8
m_{eff}	Mass effective [kg]	8
R	Radius of the circular defect [m]	8

1 INTRODUCTION

In recent years, researchers have used different active infrared thermography techniques to analyze composite structures in search of damage that could jeopardize their structural integrity (1). One of these techniques, denominated vibrotermography, requires that the material be excited through the application of vibrations and that its surface be monitored by an infrared camera for further analysis. The growing use of composite materials is observed due to their properties and in the replacement of traditionally used materials such as steel and aluminum. Therefore, their applications are increasingly present in the fields of aeronautical, civil, automotive, and aerospace (2–4).

Infrared thermography has advanced to become a reliable and cost-effective technique for non-invasive monitoring of machines and equipments (5). The heating resulting from the vibration imposed on the material changes the emission of infrared radiation that will be measured and used to build the heat map generated on the surface material. As presented by the authors in (6), the measurement of the infrared radiation intensity emitted by the body can be used both in the measurement of temperature and in non-destructive tests. Following in the same line of research, the authors in (7) performed the measurement of emissivity in composite samples of different thicknesses, showing how to calculate the unknown emissivity by applying a scientific method. Thus, the cited research shows the possibility of measuring the radiation emitted by the surface in order to record the thermal map generated on the surface of the material when using an infrared camera.

The generated temperature patterns on the surface of the material in relation to inhomogeneities or internal defects are presented with fidelity when the termography is used (8). So that, when the application of mechanical vibrations to excite the material is carried out and combined with the utilization of videothermography to view the temperature profile generated on the surface of the material, this is called vibrothermography (8).

This technique assumes that mechanical energy will be converted into heat more efficiently in a defective material than in a perfect material and can be used in two different configurations: large displacement-low frequency and small displacement-high frequency (9).

Two types of analysis can be used in infrared thermography: the first is called “passive” IRT (Infrared Thermography), which does not require an external excitation source applied to the material (10) and the second is “active” IRT, which requires an external excitation source to induce heat generation in the material (11–16). The use of mechanical ultrasonic waves in vibrothermography classifies the technique as an active method of analysis (1), and just like excitation by optical radiation or electromagnetic waves, excitation by mechanical ultrasonic waves will generate temperature gradients in the material’s surface (after the transformation of mechanical energy into thermal energy), allowing the

thermal radiation emitted to be recorded using an infrared camera (1).

In relation to the damage present in the materials, these may have been introduced during the production process, during a work cycle, or accidentally produced during the maintenance period. In order to be able to efficiently detect damage, it is necessary to know, in addition to the types and characteristics of the damage, the mechanisms of heat generation that are manifested during the excitation of the material. The analysis can be performed analytically, numerically, experimentally, or by performing a comparison between them, evaluating both the detectability presented by the technique and the characterization of the damage present in the structure. In order to increase the detection efficiency, methods of image processing can be used that allow the elimination of noise and various interferences.

Figure 1 shows a schematic illustration of the vibrothermography technique, in which the damage in the specimen is detected by measuring the radiation emitted on the material surface with an infrared camera properly positioned to sweep all surfaces of the material. The specimen, when mechanically excited at a predetermined point, shows a bigger temperature variation in the region of the damage.

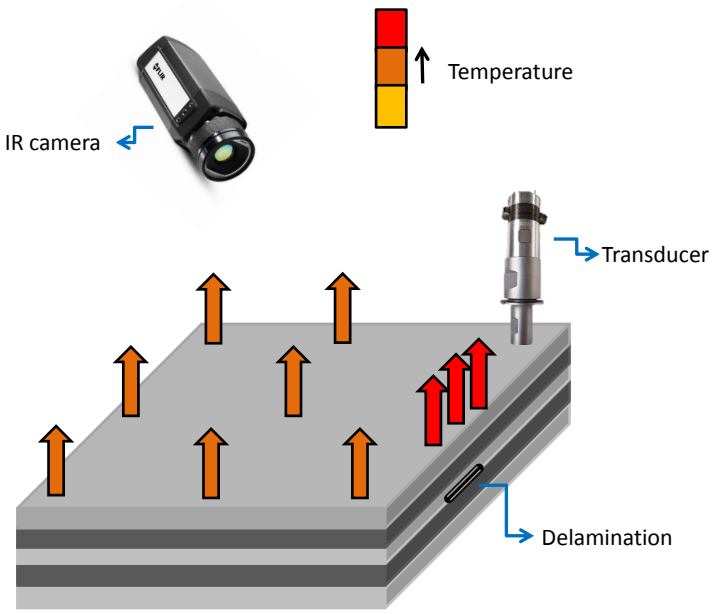

Figure 1 – Schematic illustration of heat generation in a damage.

Over the years, the technique of vibrothermography has received several contributions that have permitted its development and resulted in a greater applicability of the technique to different types of materials (17–26). It is also noted that since the beginning of the studies, the heat generation form has been of interest to the researchers. In their studies, (27) evaluated the question of how heat is generated when materials are exposed to vibratory excitation. In addition to developing a greater understanding of

the mechanisms of heat generation in the mechanically excited sample, they also got a better understanding of the way in which energy dissipation occurs in laminated materials reinforced with continuous fibers when cyclically excited, which was attributed to the viscoelastic effects and the structural dissipation as the greatest contributors to the creation of temperature patterns. For the authors in (28), it was presented that, among the forms of heat generation present in the composite materials of polymeric matrices, viscoelastic dissipative hysteresis is the most responsible for the process, being the level of tension or strain at which the sample is deformed and the cyclic frequency at which the mechanical load is applied the two most significant parameters in generating the heat patterns in the sample. In their studies, the authors of (29) presented an equation for composite thin plates that describes the different mechanics of heat transfer during the vibrothermography test, in addition to performing experimental tests to evaluate impact damage in composite materials, using a computer software program for digital processing of thermograms as a final tool. Therefore, it will be evident that the technological advance presented in recent research is improving the techniques started years ago, that is possible through the advancement of infrared cameras, the mechanisms of applying the excitation, and the post-processing mechanisms.

1.1 RESEARCH OBJECTIVES

The main objective of this work is the detection of damage in composite structures using vibrothermography, using both numeric and experimental analyses. The specific objectives are:

- Synthesize the main concepts, methods, and analyses of vibrothermography applied to composite structures, pointing out modern trends.
- Evaluate the possibility of detecting damage such as delaminations in composite structures using vibrothermography.
- Use of numerical analysis, by Finite Element Method (FEM), to detect damage using vibrothermography;
- Evaluation of heat generation in the structure during the application of different types of signals and mapping of the temperature profile generated on the surface;

1.2 DISSERTATION OUTLINE

The dissertation is organized as follows:

- Chapter 1, Introduction: i)Research Objectives, ii)Dissertation Outline;
- Chapter 2, Theoretical Review: i) Damage Detection in Composite Materials Using Vibrothermography, ii) Heat Generation Mechanisms, iii) Vibrothermography Signals, iv) Types of Analysis Applied in Vibrothermography, and v) Signal Processing Applied in Vibrthermography.
- Chapter 3, Methodology: i) Numerical Analysis, ii) Experimental Analysis.
- Chapter 4, Results and Discussion: i) Numerical Analysis, ii)Experimental Analysis.
- Chapter 5, Conclusion.

2 THEORETICAL REVIEW

In an attempt to present the latest research on vibrothermography in a more compact way, some topics will be described. It will present ways of generating damage in composite structures, low or high energy impacts, types of defects found, some heat generation mechanisms, types of signals applied, types of analysis used, and finally an approach to signal processing available and used in order to increase the efficiency of damage detection in the structure.

2.1 DAMAGE DETECTION IN COMPOSITE MATERIALS USING VIBROTHERMOGRAPHY

The analysis of the composite material structure in search of damage can be performed using vibrothermography or other techniques that use or do not use infrared thermography. The mapping that goes beyond the surface of the material allows different types of damage to be detected, which guarantees the use of the components or structures with greater safety, allowing the advancement of the application of composite materials in the manufacturing and development sectors.

The detection of impact damage is a major concern for the industry, as there is the possibility that there are no marks on the surface of the structure indicating its collision with some object during maintenance or during a work cycle, creating uncertainty about releasing the component or structure for use in a new cycle. Considering the different environments to which the structure will be exposed, the studies carried out can consider two types of impacts: low- or high-speed impacts, also known as low- or high-energy impacts, respectively. Known as BVID (Barely Visible Impact Damage), the damage is difficult to identify visually but is generated by low-velocity impacts and is responsible for inducing defects such as delamination, detachment, or cracks in the structure matrix. The existence or lack of visually detectable marks on the surface of the structure further evidences the need to detect these types of damage, making it important to use techniques such as vibrothermography to assess the structural integrity of the material.

From Table 1 it is observed that different authors have carried out research on damage generated by low-energy or low-speed impacts, to structures composed of GFRP (Glass Fiber Reinforced Polymer), PCM (Polymer Matrix Composite), and CFRP (Carbon Fiber Reinforced Polymer). The difficulty in detecting these types of damage has drawn the authors' attention in recent years, in contrast to high-energy or high-velocity impacts, which allow for visual identification of the impact suffered. Figure 2 shows an example of impactors used to generate BVID in glass E-fabric-reinforced 14-layered epoxy composite

material.

Table 1 – Impactors used in the generate BVDI.

REFERENCE	IMPACT	IMPACTORS	MATERIAL
(30)	low velocity	spherical, cylindrical and half-spherical	GFRP and CFRP
(31)	low velocity	Hemispherical and ogival	PCM
(32)	low velocity	Hemispherical	Carbon/epoxy plate
(33)	low power	Free-falling hammer	CFRP
(34)	low velocity	Hemispherical	CFRP and GFRP
(35)	low energy	Spherical, con. and cylindrical	GFRP and CFRP
(36)	low velocity	Hemispherical	CFRP
(37)	low velocity	Hemispherical	CFRP
(38)	low energy	(−)	CFRP
(39)	low power	Hemispherical	CFRP
(40)	low power	Free-falling hammer	CFRP

Figure 2 – Impactors used to generate BVDI in plate of composite material (Adapted from (31)).

In addition to the BVID, the study of damage in composite materials can also be carried out through the production of the structure with pre-established damage or through the insertion of these after the material is produced. This type of analysis allows the study of damage with different characteristics, sizes, orientations, and depths. Delaminations, notches, FBH (Flat Bottomed Hole), or cracks can be induced in the materials and analyzed to assess the vibrothermography technique's ability to detect damage. Table 2 presents studies carried out by different authors to identify different types of previously induced damage in the structures.

From Table 2, it is observed that, beyond the barely visible impact damage shown in Table 1, delaminations generated or induced in composite materials, which are not the result of impact damage, are responsible for most studies involving damage detection by application of the vibrothermography technique.

Table 2 – Damage present in the composite materials being studied

REFERENCE	MATERIAL	DAMAGE
(41)	CFRP	Cracks
(42)	PCMs	Notches
(43)	Glass E-Fabric Reinforced 14-layered epoxy	FBHs
(44)	CFRP	Micro Porosites
(45)	CFRP	FBHs
(46)	CFRP	Delamination
(47)	Carbon fibre prepreg laminate	Delamination
(48)	CFRP	Delamination
(49)	E-Glass/Epoxy laminated	Delamination
(50)	CFRP	Delamination
(51)	Polymenthylmethacrylate structure	FBH
(52)	Aluminium honeycomb with face sheet	Delamination graphite epoxy
(53)	CFRP	Small chacks and voids
(54)	CFRP	Delamination
(55)	Glass/epoxy 2d woven	Micro-cracking
(56)	CFRC	Delamination

2.2 HEAT GENERATION MECHANISMS

In order for energy loss to exist, that is, for an amount of energy to be dissipated during excitation of the material, it is necessary that in the analytical representations, damping or dissipative terms are introduced in a linear theory (8). Thus, among the dissipative mechanisms identified in materials, some can produce heat patterns observable through the vibrothermography technique, such as viscoelastic dissipation, standing wave resonant dissipation, plastic slip, the rubbing and clapping of adjacent surfaces, and also "local vibrations" of material phases or defect surfaces(8).

Therefore, to detect damage in composite materials, it is essential to know the mechanisms of heat generation that manifest during the excitation of the material. Understanding their importance, some studies were carried out addressing two of the mechanisms cited previously: the first that considers the heat dissipation by viscoelastic effects, defined as viscoelastic heating or SHVT (Self-Heating Vibrothermography-Based), and the second that considers the amplification of the damage local vibrations due to the characteristic frequency used to excite the specimen, defined as LDR (Local Defect Resonance).

Regarding the mechanism that considers viscoelastic heat dissipation, the authors of (57) showed that viscoelastic heating manifests itself when the specimen is vibrated intensely, so that high stress concentrations manifest themselves by generating heat around the damage. Theoretical and experimental studies were carried out by (58) to evaluate the effect of high heating resulting from energy dissipation in viscoelastic materials when they are exposed to vibration. In (59), self-heating temperatures on the surfaces of the bodies

were obtained after carrying out fatigue tests, and the critical temperature at which the mechanical degradation of a composite structure begins was shown.

When analyzing the amplification of local vibrations, the author (60) discovered that the presence of a defect reduces the local stiffness for a given mass of material, resulting in a resonance frequency characteristic of the defect, i.e., when exciting the material at the LDR frequency, the defect receives energy from the applied mechanical wave, resulting in a greater temperature variation.

The characterization of the defect (type and location) and the response of the material exposed to mechanical excitation (thermoelastic effect, thermoplastic effect, and heat generation by friction), are essential for the assembly of the equation that will allow the calculation of the generated heat in the defect.

An example of the analysis involving a heat generating mechanism is shown in (51), (60) and (61), where the equations for LDR frequency used for present flat-bottom hole defects can be found. From Equation 2.1, used for different types of defects, the "natural frequency of the defect" (f_{LDR}) is calculated as a function of the effective mass and stiffness, m_{eff} and k_{eff}, respectively.

$$f_{LDR} = \frac{1}{2\pi}\sqrt{\frac{k_{eff}}{m_{eff}}} \tag{2.1}$$

The effective stiffness and mass (Equations 2.2 and 2.3, respectively), which are functions of the bending stiffness (D) (Equation 2.4) and residual mass of the FBH (m) (Equation 2.5), are substituted in the Equation 2.1.

$$k_{eff} = \frac{198\pi D}{R^2} \tag{2.2}$$

$$m_{eff} = 1.8m \tag{2.3}$$

$$D = \frac{Ed^3}{12(1-\upsilon^2)} \tag{2.4}$$

$$m = \rho\pi R^2 \tag{2.5}$$

where, R is the radius of the circular defect, d is the residual wall thickness of the FBH, is the modulus of elasticity of the specimen, υ is the Poisson's ratio and ρ is the density.

Finally, the frequency of the defect presented in Equation 2.6 is used for the excitation of the material, allowing a greater amount of energy to be concentrated in the defect.

$$f_{LDR} = \frac{1.6}{R^2}\sqrt{\frac{Ed^3}{12(1-\upsilon^2)}} \tag{2.6}$$

Thus, to present other recent studies that use heat generation mechanisms to perform damage detection in composite materials, Table 3 was constructed.

Table 3 – Different mechanisms of heat generation.

REFERENCE	MATERIAL	HEAT GENERATION
(31)	Glass E-Fabric Reinforced 14-layered epoxy	Self-Heating
(43)	Glass E-Fabric Reinforced 14-layered epoxy	Self-Heating
(45)	CFRP	Local Defect Resonances
(54)	CFRP	Local Defect Resonances
(57)	CFRP	Viscoelastic Heating
(60)	PMMA	Local Defect Resonances
(62)	Glass E-Fabric Reinforced 14-layered epoxy	Self-Heating
(63)	Glass E-Fabric Reinforced 14-layered epoxy	Self-Heating
(64)	CFRP	Local Defect Resonances
(65)	CFRTP	Self-Heating

As presented in Table 3, most authors have directed their research to the analysis of damage using Local defect Resonance and Self-Heating. The use of Local Defect Resonance requires that the frequency of damage resonance at which the body should be excited be determined, making it interesting to use tools to help determine this frequency. Self-heating, on the other hand, requires that the resonant frequencies acquired from the specimen under analysis be used to build a harmonic or multi-harmonic signal that will be applied to the specimen for the effect of Self-Heating to be possible.

2.3 VIBROTHERMOGRAPHY SIGNALS

When analyzing the vibrothermography technique, the possibility of varying the characteristics of the applied signals, that is, the use of signals with high or low frequencies, periodic or non-periodic, harmonic or multi-harmonic, is essential for the technique to be used efficiently. Thus, as important as knowing the mechanisms of heat generation that are responsible for inducing different profiles of temperature on the surface of the material during sample excitation is, knowledge of the natural frequencies presented by the specimen is also important to modeling the signal applied to the specimen. Therefore, the possibility of direct application of signals with frequencies available in the equipment used, seeking an excitation of the damage by sweeping the entire range of available frequencies, and performing a modal analysis allows the resonant frequencies to be obtained, which makes it possible to apply the frequency itself or the construction of multi-harmonic signals (from the resonant frequencies) in the vibrothermographic analysis.

As described, the natural frequencies of the specimen can be used to compose the excitation signal applied in the experiment. Thus, Figure 3 shows the use of these frequencies in the excitation of a beam, which has beeb manufactures with 9 equidistant notches with a depth of 0.5mm and distances of 25mm from each other introduced into

the upper surface of the specimen, where the greatest efficiency in damage detection can be seen when using the signal composed of harmonic signals corresponding to the 1st, 2nd and 3rd natural vibration frequencies.

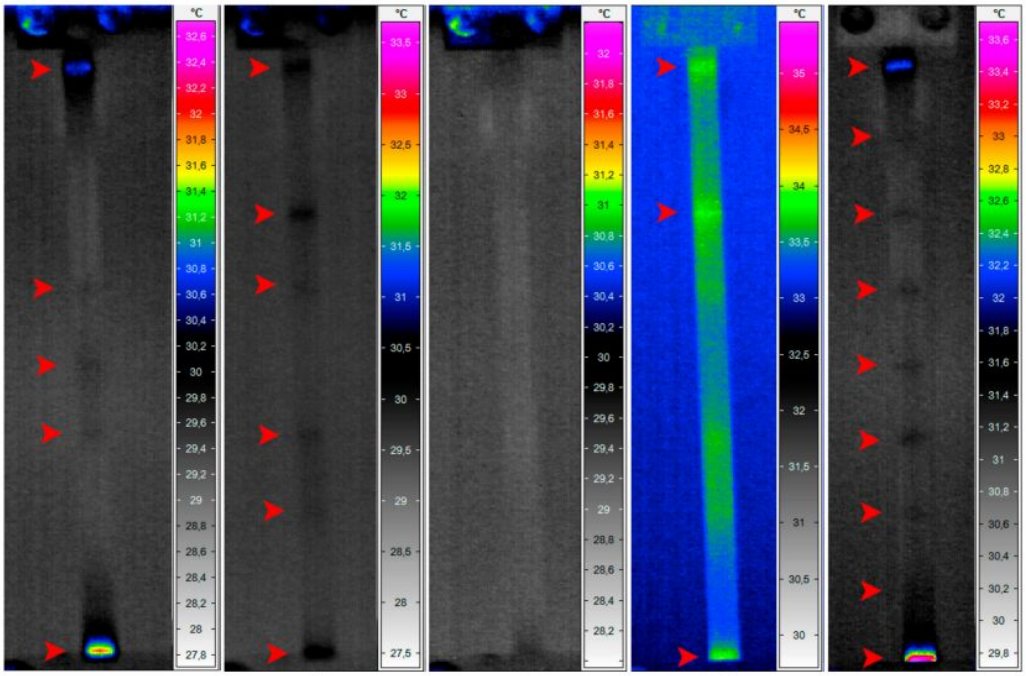

Figure 3 – Temperature distribution during loading on: a) first harmonic; b) second harmonic; c) third harmonic; d) second and third harmonics; and e) first, second, and third harmonics(Adapted from (62)).

In order to present the signals used in research, Table 4 allows the reader to know the signals applied in the detection of damage. It is noted the use of signals of low- or high-frequency and a combination of the natural frequencies of the specimen.

Table 4 – Different types of signs applied in Vibrothermography.

REFERENCE	SIGNAL
(30)	15, 20 and 30 kHz ultrasonic excitations frequencies
(31)	Multi-harmonic signals composed from harmonics corresponding to the acquired resonant frequencies
(32)	A 28-kHz sinusoidal signal
(34)	The system is able to perform an acoustic source having a driving frequency of 20 kHz
(37)	Vibrational excitation was applied at the selected LDR frequency of 91.3 kHz, and was modulated at different AM frequencies 0.1, 0.075 and 0.05 Hz
(41)	Burst of ultrasound waves (15 - 25 kHz, 2200 W) at a modulation frequency of 0.2 Hz and with amplitude modulated between 10-30 of maximum power
(43)	For frequency range of 0-1250Hz, the collected resonant frequencies were used for a construction of a signal
(44)	A burst of ultrasound wave (20 kHz, 2200 W) at a modulation frequency of 0.25 Hz and with amplitude modulated between 10% and 30% of maximum power
(50)	Ultrasound frequency 15–25 kHz, Waveform modulation or pulsed, minimum modulation frequency 0.1 Hz, amplitude 0 to 100%
(54)	A point by point(every 0,2 kHz) sinusoidal vibrothermography has been conducted in the range 8-27kHz
(56)	Ultrasound frequencies ranging from 15 to 25 kHz (optimum ultrasound frequency of 19.75 kHz)
(57)	Typical vibrational frequencies used are in the 20-40 kHz range
(58)	Multi-frequency mode with frequencies of: 1, 10, 20, and 50 Hz with a constant amplitude of 80 lm and maximal force of 5 N
(59)	The specimens were cyclically loaded with an excitation frequency of 30kHz
(62)	The modal analysis was performed in the frequency range of 0–1500Hz with the frequency resolution of 1.5625 Hz, and after were used multi-harmonic signals corresponding with multiple natural frequencies
(63)	The classical modal analysis was realized, and after was utilized the harmonics with the acquired resonant frequencies.
(64)	Linear burst chirp signal (i.e. fast swept sine followed by a zero signal for 10%
(66)	Frequency 5kHz
(67)	frequency 6 kHz and a signal peak-to-peak amplitude equal to 12 V
(68)	A chirp signal was created for the excitation, which swept from 50 to 1000 Hz

Looking the Table 4 , it is possible to note that many of the studies use multi-harmonic signals to excite the material. So that the utilization of natural frequencies in the composition of the multi-harmonic signal presents itself as essential and powerful to excite all structure of the specimen, which results in a greater number of damages detected, increasing the efficiency of the technique. In relation to the other characteristics of the signals of excitation, the utilization of larger or smaller amplitudes can be used to finish the modeling of the signal; it is important to choose amplitudes that, when associated with natural frequencies, can generate the excitation of the damages and do not result in the aggravation of the damages present in the structure.

2.4 TYPES OF ANALYSIS APPLIED IN VIBROTHERMOGRAPHY

The damage present in the materials can be detected analytically, numerically, experimentally, or by carrying out a comparison between two or more methods of analysis. Because it makes use of approximations or considerations, numerical analysis produces results that are close to reality (35). Analytical analysis provides a precise result but requires a more complex formulation of the phenomenon (37). As for the experimental analysis, it is necessary to have a specific setup for mapping damage through the application of the vibrothermography technique (1, 44, 69, 70). Therefore, whatever method is used, damage detection is realized by analyzing the temperature profile generated on the surface of the specimen after mechanical excitation. The presence of temperature gradients indicates a non-uniformity in the material, turning on a warning sign for a region in the highlight. Different from the experimental analysis that captures images on the surface of the material after application of the vibration in the specimen, the analytical and numerical analysis makes use of equations that relate point by point the characteristics of the materials that compose the specimen with the physical phenomena existing to generate these temperature gradients on the surface of the material.

Figure 4 shows an example of a setup experiment where the images captured by an infrared camera are sent to the computer after mechanical excitation is applied to the specimen. Figure 5 (Adapted from (35)), shows an example of FE damage simulation and vibrothermography-detect damage for an impact energy of 13 Joules.

The experimental analysis method is the most commonly used in recent studies using vibrothermography, which highlights the importance of identifying damage in samples of structural components. The positioning of the elements that will apply the excitation to the sample (transducer and horn), the positioning of the infrared camera that will allow the entire surface of the material to be framed, and the sending of the captured images to the computer must all be done in parallel with a signal generator and a power source for this analysis.

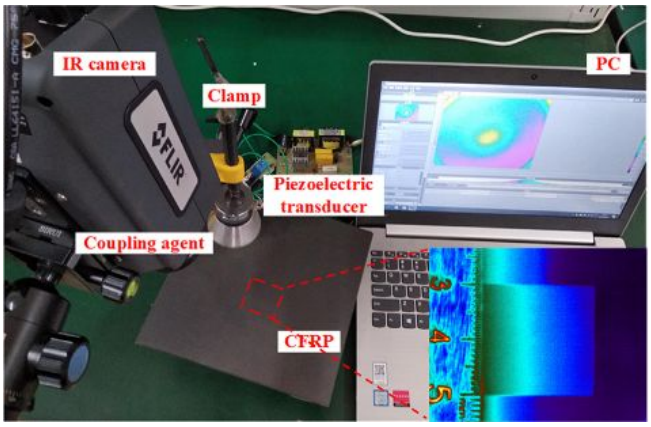

Figure 4 – Example of experimental setup (Adapted from (33)).

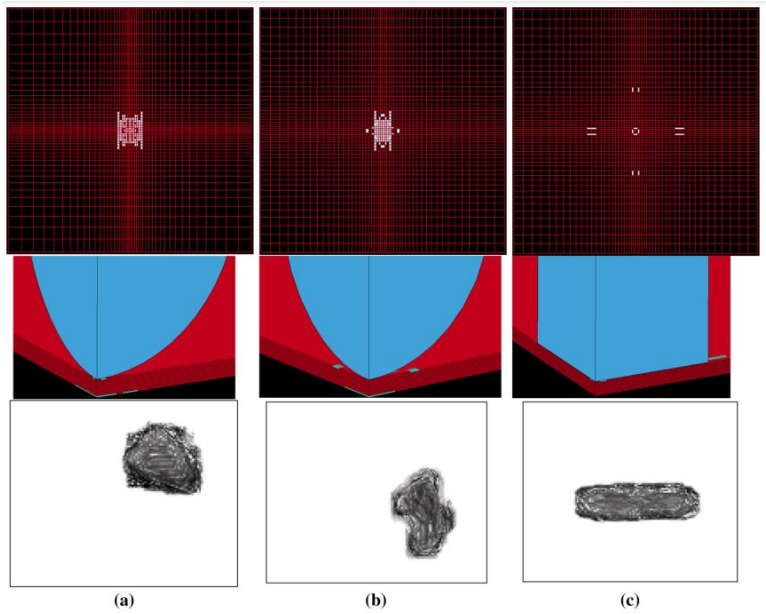

Figure 5 – FE damage simulation and vibrothermography−detect damage using strikers: a) spherical, b) half-spherical and c) cylindrical (Adapted from (35)).

As shown in Figure 6, the application of active infrared thermography in non-destructive testing can be based on different physical principles (optical radiation, acoustic/ultrasonic wave propagation, electromagnetic radiation for dielectric materials, and thermo-resistive radiation for composite materials) as the thermal source for the damage detection techniques presented. The acronyms in Figure 6 are listed in Table 5 for the reader's complete understanding. Analyzing the central branch shown in blue in the flowchart in Figure 6, the vibrothermography technique is presented as a branch of UST (highlighted in red) and is divided into lock-in vibrothermography (or amplitude modulated VT), in which the signal is applied periodically over a short period of time, i.e., the signal is generated at specific time intervals, and burst vibrothermography, in which the signal is applied pe-

riodically over a short period of time, i.e., the signal is generated at specific time intervals (Figure 7). This technique can be found in several studies that have shown that lock-in vibrothermography and burst vibrothermography generally depend on high excitation frequencies (ultrasound) and the phenomenon of wave propagation (71–75).

Table 6 presents the studies that used different types of analysis to identify damage in samples of composite materials. This information is presented together with the method of analysis used, that is, whether a "passive" or "active" IRT, a mathematical model, or an analysis was carried out using the finite element method.

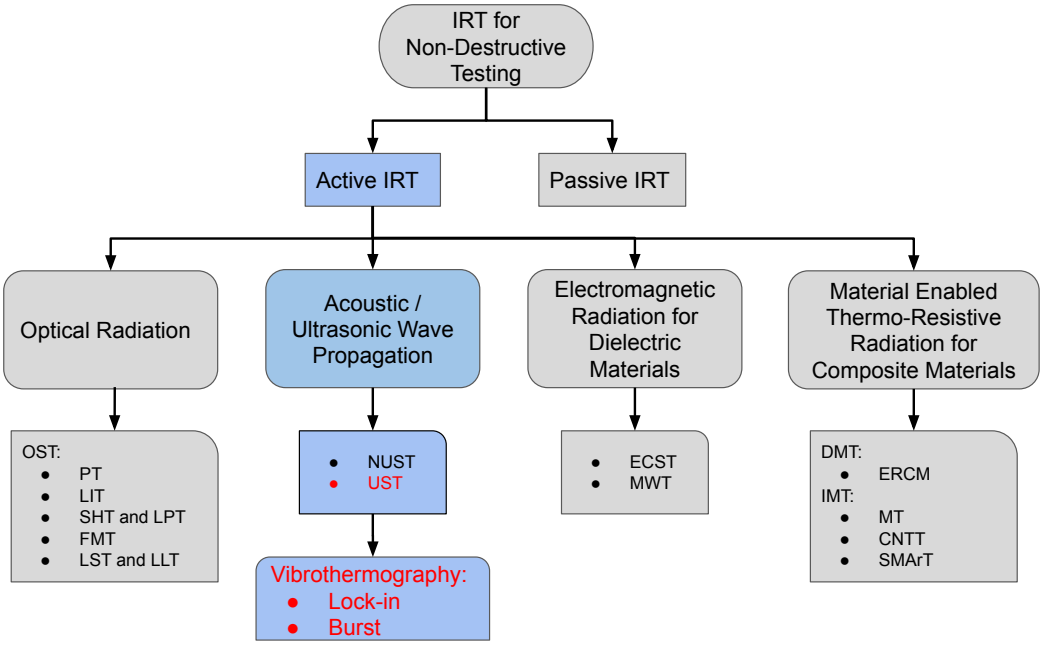

Figure 6 – IRT for Non-Destructive Testing (Adaptated from (1)).

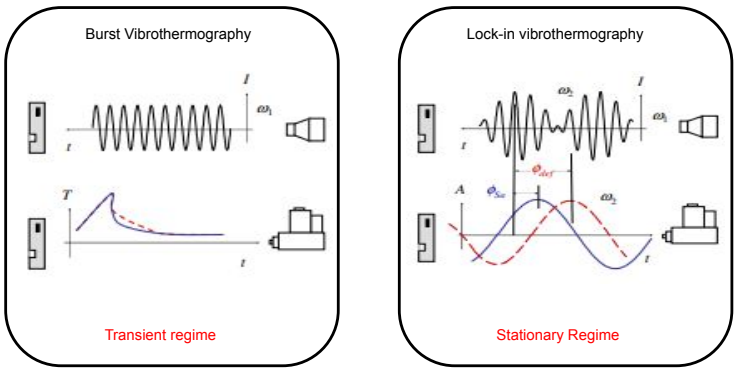

Figure 7 – Burst and Lock-in vibrothermography (Adapted from (76)).

From Table 6, we can see the current trend in both the use of active methods and the performance of experimental analyses. The use of an energy source that allows a greater

Table 5 – Acronyms used for IRT techniques.

ACRONYM	REFERENCE
OPTICALLY STIMULATED THERMOGRAPHY (OST)	
PT (Pulsed Thermography)	(77)
LIT (Lock-in Thermography)	(78)
SHT (Step-Heating Thermography)	(79)
LPT (Long Pulse Thermography)	(80)
FMT (Frequency Modulated Thermography)	(81)
LST (Laser-Spot Thermography)	(82)
LLT (Laser-Line Thermography)	(83)
ACOUSTIC / ULTRASONIC WAVE PORPAGATION	
UST (Ultrasonic Stimulated Thermography)	(84)
NUST (Nonlinear Ultrasonic Stimulated Thermography)	(85)
ELETROMAGNETIC RADIATION	
ECST (Eddy Current Stimulated Thermography)	(86)
MWT (Microwave Thermography)	(87)
MATERIAL ENABLE THERMO-RESISTIVE	
DMT (Direct Material-Based Thermography)	
ERCM (Eletrical Resistance C. M. Coupled to Thermography)	(88)
IMT (Indirect Material-Based Thermography)	
MT (Metal-Based Thermography)	(89)
CNTT (Carbon Nanotubes-Based Thermography)	(90)
SMArt (Shape Memory Alloys-Based Thermography)	(91)

generation of heat in the damage when the material is excited makes the use of the active method in the analysis of the materials more attractive. Thus, post-processing methods can be used to increase the efficiency of the technique when processing the data produced in the test.

2.5 SIGNAL PROCESSING APPLIED IN VIBROTHERMOGRAPHY

The data obtained during the application of the vibrothermography technique may not allow damage to be identified or characterized. The researchers seek to increase efficiency in the detection and characterization of the damages using methods to post-process the data, which would provide better results.

Some factors hindering the detection and characterization of damage, such as the low quality of the images captured by the infrared camera after the excitation of the sample, the presence of noise from the process of excitation or heating, and the demand for large storage spaces, highlight the need for post-processing. Therefore, post-processing of the data can be used as a final or intermediate step.

In this context, techniques like PCA (Principal Component Analysis), ICA (Indepen-

Table 6 – Type of analysis applied

REFERENCE	TYPE OF ANALYSIS	METHOD
(30)	Experimental	Active
(33)	Experimental	Active
(34)	Experimental	Active
(35)	Numerical; Experimental	Finite Element Model; Active
(37)	Analytical and Experimental	1D analytical model; Active
(43)	Experimental	Active
(44)	Experimental	Active
(45)	Experimental	Active
(46)	Numerical and Experimental	Finite Element Model; Active
(48)	Experimental	Active
(49)	Numerical and Experimental	Finite Element Model; Active
(50)	Experimental	Active
(57)	Experimental	Active
(62)	Experimental	Active
(63)	Experimental	Active
(64)	Numerical; Experimental	Proposed Algorithm; Active
(66)	Experimental	Active
(67)	Experimental	Active
(68)	Experimental	Active
(70)	Experimental	Active
(76)	Experimental	Active
(92)	Numerical and Experimental	Finite Element Model; Active
(93)	Experimental	Active
(94)	Experimental	Active
(95)	Experimental	Active

dent Component Analysis), PCT (Principal Component Thermography), PPT (Pulsed Phase Thermography), FT (Fourier Transform), PSD (Power Spectral Density), or OMA (Operational Modal Analysis) allow for data post-processing, which improves the effectiveness of damage detection.

In order to exemplify the post-processing, Figure 8 shows the use of the PCA method, which allows a statistical analysis of the data generated during the experiment. Thus, according to Figure 8, four snapshots were presented, identified with their respective capture times defined during the vibrothermographic test. When using the PCA method, four of the 181 images that best presented the thermal patterns of interest during the experiment were presented. However, the method was not able to completely separate and extract the thermal patterns in the regions of interest.

The use of mathematical methods in post-processing allows the analysis of data obtained during the tests, providing an increase in detection efficiency and an improvement in the characterization of damage. The choice of method to be used must consider the characteristics of the data; for example, the reconstruction of the source signals, the reduction of the number of variables, followed by the creation of new variables, or the

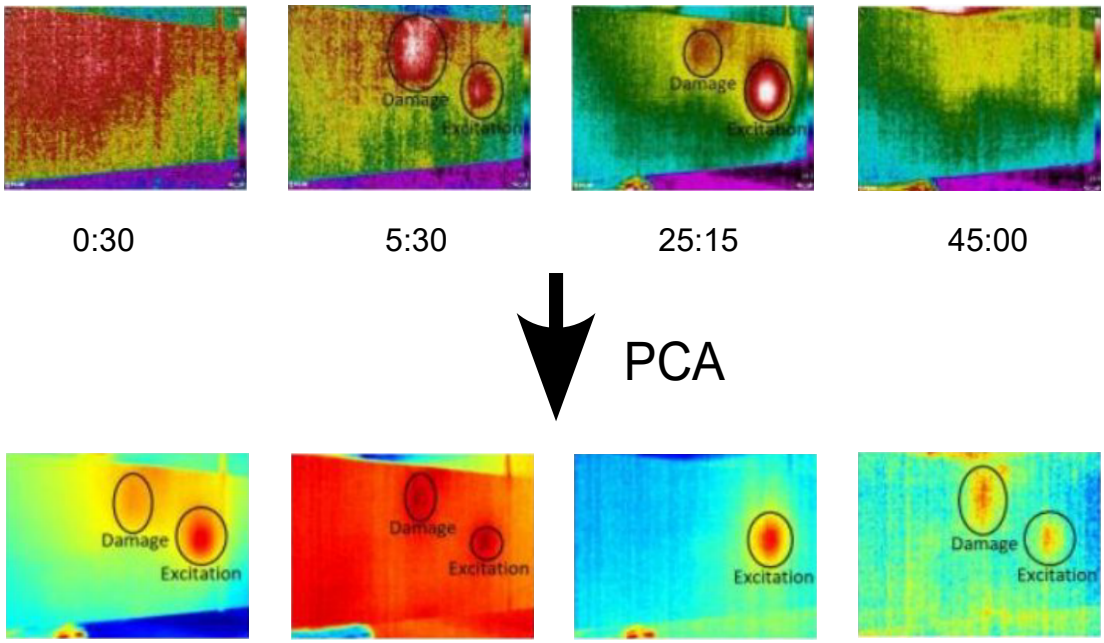

Figure 8 – Post-processing using PCA (Adapted from [97]).

identification of the modal properties of the structure based on data can be performed for vibration.

Table 7, show the subjects of each post-processing used in damage characterization.

Therefore, analyzing the methods used, it can be seen that the data presented in the algorithms accelerates both the extraction of parameters and the analysis of the data obtained. As described in Table 7, there are many methods available to perform post-processing, and the use of some of them in the same experiment allows us to define which was the most efficient for that particular application. It should be noted that in addition to the techniques and methods described, other non-destructive testing techniques, such as PCT and ICT can be used for post-processing in vibrothermography.

Table 7 – Type of method applied.

REFERENCE	POST-PROCESSING	RESUME
(33)	FT	The conversion of data from the time domain to the frequency domain was obtained by applying the FT to each pixel of the thermal sequence.
	ICA	The elimination of noise with improved visibility of damage.
(45)	PCA	Is a multivariate technique which reduce the dimensionality of a dataset.
	PSD	Gives the vibrational energy averaged over a frequency band with bandwidth.
	OMA	Extract the resonance frequencies from the full-field broadband vibration.
(63)	Statistical characteristics	Calculation of a statistical feature value based on all values from a considered sequence of thermograms.
	Temperature profile trend estimation	Calculation of values of parameters connected with trends of temperature profiles in the thermogram's pixel coordinates.
	Similarity maps	Producing an image with similarity coefficient values between chosen thermograms.
(94)	PCT	Used in the processing of infrared images, this technique extracts the image features, reducing undesirable signals.
	PPT	Extract amplitude and phase information from the raw thermal data.
(96)	ICA	Superior results compared to PCA, allowing better identification.
(97)	Adaptive algorithm	Evaluate the performance of the image compression process, acting in the identification and location of the affected regions in a more significant way.
(98)	PCA	Was used to select effective parameters and reduce the information dimension.

3 METHODOLOGY

As seen in the literature, the region at the knowledge frontier that most needs to be explored in relation to vibrothermography concerns numerical analysis and the type of signal used to excite the specimen. The numerical analysis using viscoelastic characteristics allows us to determine how this mechanism can influence the temperature variation on the material surface. As for the change in the characteristics of the signals used, the longer the time exposed to maximum stresses, the greater the changes in the internal heat generation of the structure.

3.1 NUMERICAL ANALYSIS

The proposed numerical analysis aims to show the temperature profile generated on the surface of the structure after the application of cyclic loads, whose temperature increment generated for each node of the mesh proposed for the structure is related to the loading intensity (maximum stress induced per cycle and excitation frequency), the physical (specific mass), mechanical (loss modulus) and, thermal properties (thermal conductivity coefficient) presented by the specimen studied. Thus, after the numerical simulations, the presence of a temperature gradient that indicates the presence of damage in the structure eliminates the need to continue with the simulation, but the non-detection of the damage from temperature profile requires the modification of the excitation signal to perform new simulations. In order to better present the methodology used in the numerical analysis, the main stages of the process are presented in Figure 9.

After modeling the structure and applying the boundary conditions, the frequencies obtained in the modal analysis (first simulation) can be used to compose the excitation signal, which will be applied to cyclically excite the structure. In the second simulation, the mechanical properties and the frequency chosen to model the excitation signal are used to calculate the maximum stress generated in each node of the beam per excitation cycle. Also in the second simulation, the temperature increment generated at each node of the structure is calculated when the value of the loss modulus measured experimentally is added to the simulation. Thus, when the numerical simulation is carried out using the temperature increment for each node of the structure to generate the temperature profile on the surface of the material (the third simulation), whether or not the pre-induced damage is detected will imply the end of the simulation or a change in the excitation signal for a new simulation. If there is a necessity to change the excitation signal, the frequency value will be modified to do a new simulation.

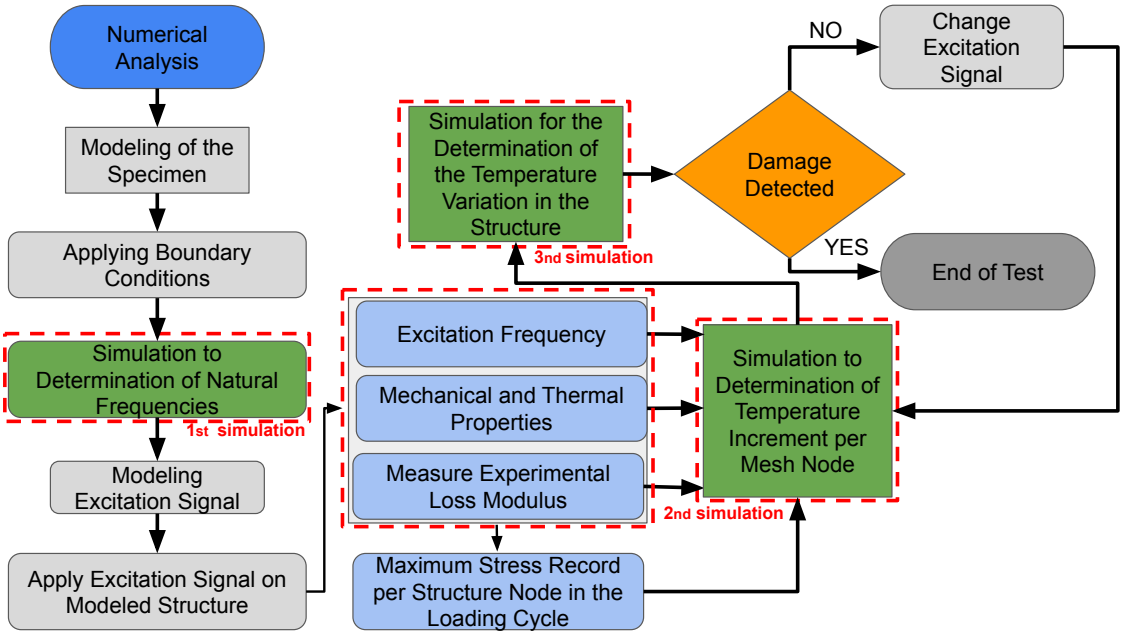

Figure 9 – Methodology used to perform the numerical analysis.

3.1.1 Modeling and Boundary Condition

The design of the sandwich beam was performed using computer-aided engineering (CAE) software, which allowed the modeling and numerical analysis. This is composed of the materials Prepreg and Rohacell Hero 71®, whose configuration presents the Prepreg material at the upper and lower faces and Rohacell Hero 71®, located in the middle of the structure, as shown in Figure 10. In the structure, each laminate prepreg shows three layers that are oriented 0^{o} and 90^{o} in relation to *x-axis*.

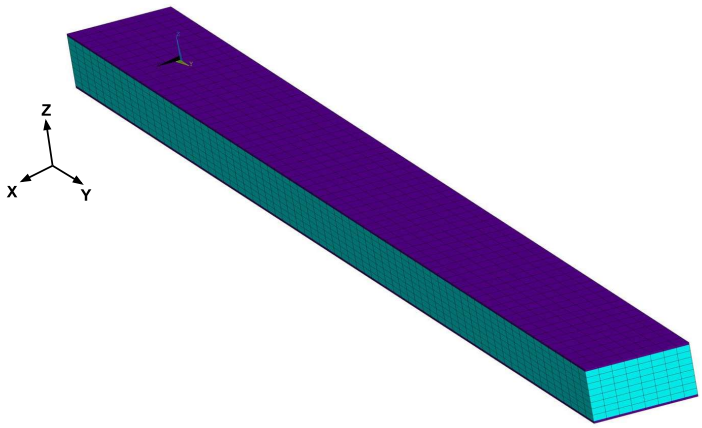

Figure 10 – Sandwich beam compose Prepreg in the skin and Rohacell Hero 71®, in the core.

The elements used to build the sandwich beam were: SOLID186, which has quadratic displacement behavior and a high deformation capacity; SHELL281, which can be applications for modeling composite shells or sandwich construction (Figure 11 (Adapted from (99))).

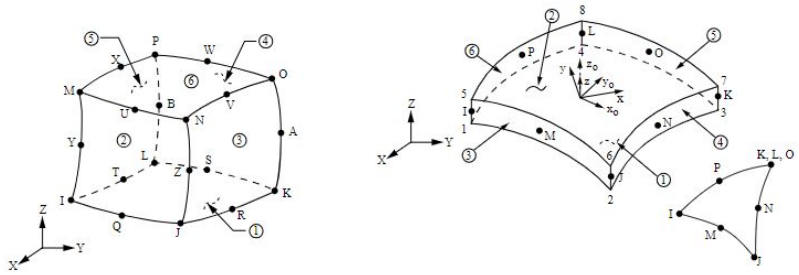

(a) (b)

Figure 11 – Elements used in the beam: a) core (SOLID 186), b) skin (SHELL 281).

However, with this configuration, the simulation time was too long, so the elements were changed. The new sandwich beam construction elements were SOLID185 that is used for 3-D modeling of solid structures and SHELL181 that suitable for analyzing thin to moderately-thick shell structures, which had a small influence on the results (Figure 12 (Adapted from (99))).

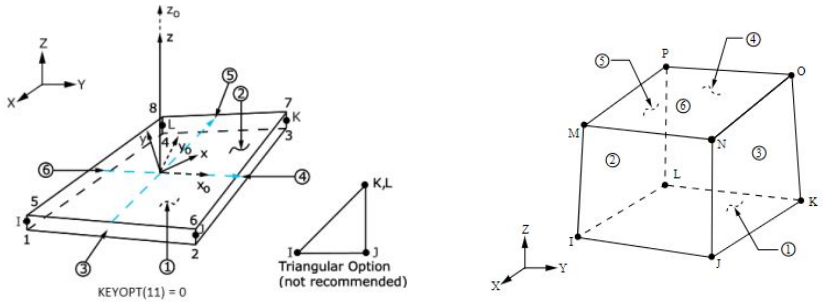

(a) (b)

Figure 12 – New elements used in the beam: a) skin (SHELL 181), b) core (SOLID 185)

The dimensions of the sandwich beam and the properties of the materials are presented in the Tables 8 and 9, respectively.

Table 8 – Dimensions of the sandwich beam.

DIMENSION	VALUE	UNIT
Lenght	0.360	m
Widht	0.024	m
Thickness	0.0147	m

To start the analysis, some boundary conditions must be applied, i.e., the region of cantilever and the point of application of the cyclic loading must be known. For this

Table 9 – Properties of the materials.

MATERIAL	PROPERTIES		VALUE	UNIT
Rohacell Hero 71®	Tensile Modulus	E_T	123	MPa
	Compressive Modulus	E_c	48	MPa
	Shear modulus	G	28	MPa
	Density	ρ	75.0	kg/m^3
	Poisson's Ratio	ν	0.25	-
Prepreg	Tensile Modulus 0°	E_T	62.9	GPa
	Tensile Modulus 90°	E_c	59.2	GPa
	Shear modulus	G	2.96	GPa
	Density	ρ_1	1510	kg/m^3
	Poisson's Ratio	ν_{12}	0.024	-
	laminate thickness	e_1	0.001	m

purpose, Figure 13 shows the position of the cantilever at one end of the sandwich beam (localization in the coordinates axis) and the location of the damage under the carbon layer. The damage was defined by applying different mechanical and thermal properties to the elements that compose it, and its location was chosen away from the cantilever region and away from the region of application of cyclic loads to avoid the regions of higher stresses generated in the beam during loading. This choice is important both to compare the location of the temperature profile generated on the surface of the material with the location of the damage in the sandwich beam and to move the damage away from the points of higher temperature increment (this parameter will be presented at Section 3.1.4) that can make its identification difficult.

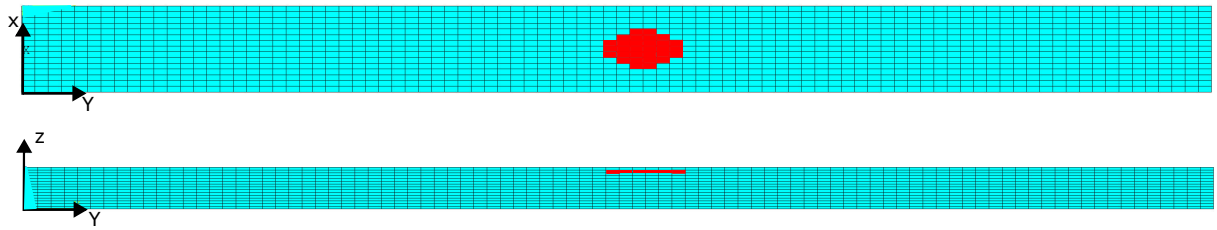

Figure 13 – Locating of the damage in the cantilever beam.

3.1.2 Definition of the Natural Frequencies

From the structure defined in Section 3.1.1, the first ten mode shapes were obtained from modal analysis, and their values are presented in Table 10. For better understanding and visualization of the mode shapes, Figure 14 show the manifestation of the mode shapes to frequencies of up to 1510.78 Hz.

According to Figure 14, in addition to the xy bending plane, the xz bending plane and y-axis torsion shapes are presented in the ten first modal shapes. Thus, For each mode shape, it is possible to use the respective frequency to excite the specimen.

Table 10 – Obtained Natural frequences.

MODE	FREQUENCY (Hz)	MODE	FREQUENCY (Hz)
1	91.48 (xy bending plane)	6	833.56 (xy bending plane)
2	177.43 (yz bending plane)	7	1006.66 (y-axis torsion)
3	286.46 (y-axis torsion)	8	1023.82 (yz bending plane)
4	296.83 (xy bending plane)	9	1151.85 (xy bending plane)
5	557.72 (xy bending plane)	10	1510.78 (xy bending plane)

In relation to the influence of the change in frequency of the signal of excitation, (100) considers to describe a physical model that exists independent of the excitation frequency, i.e., this independence allows it to be possible to do a quasi-static experiment to determine the behavior of the material after excitation. But, when using the frequencies in reference to the modal shapes, the presence of resonance generated from excitation using the natural frequencies causes bigger displacements in the structure, which is an interesting parameter to be used in the simulations.

In the first stage of the study, the use of different frequencies will be important to assess the impact of each frequency on the calculated temperature increase. Note that, due to the resonance phenomenon, i.e., the possibility of using the natural frequency value, that will create the manifestation of different displacements on the structure, characteristic of each modal response, which will generate different temperature increases due to the different stress values generated in each region of the structure.

3.1.3 Modeling Excitation Signal

In addition to the difference in frequency value, the type of excitation signal can change, i.e., the shape of the wave applied (sine, square, or triangular, for example). This signal can have the natural frequency in its composition, which can be measured from modal analysis, and the resonance phenomenon can be used to increase the displacement and consequently the energy involved during the simulation. As presented in Section 2.4, signals with different frequencies are applied to the test specimens, and in many cases, frequencies are used to excite the specimen, individually ((101)) or in combination ((58), (31), (62), (63)). Thus, to improve the analysis, three types of signals will be used (Figure 15), where in each set of simulations, waves with the same amplitude and frequency are applied.

Although they have similar characteristics, it can be seen that the square wave excites the maximum displacement in a longer time compared to the sine and triangular waves, i.e., the structure will be exposed to the maximum stress for longer. Another observation occurs when comparing the three waves, i.e., there are negative and positive stresses during the simulation, which will generate the traction-compression mechanism in the exposed structure.

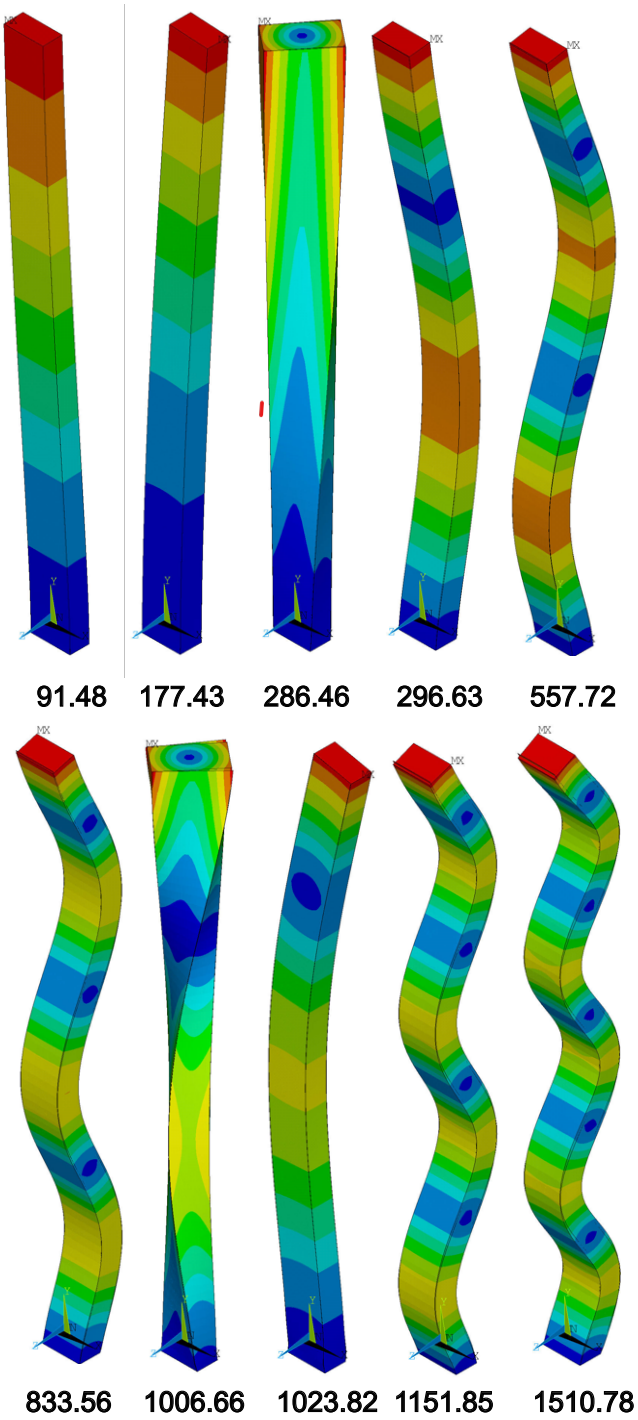

Figure 14 – First ten mode shapes (Hz).

According with (102), in a viscoelastic body, the energy involved in the total work of deformation has a part stored elastically and other part dissipated as through viscous losses. Already considering the mechanical hysteresis presented by a structure, many approaches are described for this phenomenon. The format and localization of the curve of response strain-stress used to calculate the dissipated energy are influenced by the type of signal excitation, i.e., the square or triangle waves, for example, generating change in the response strain-stress (103). For example, Figure 16 shows the stress-strain response

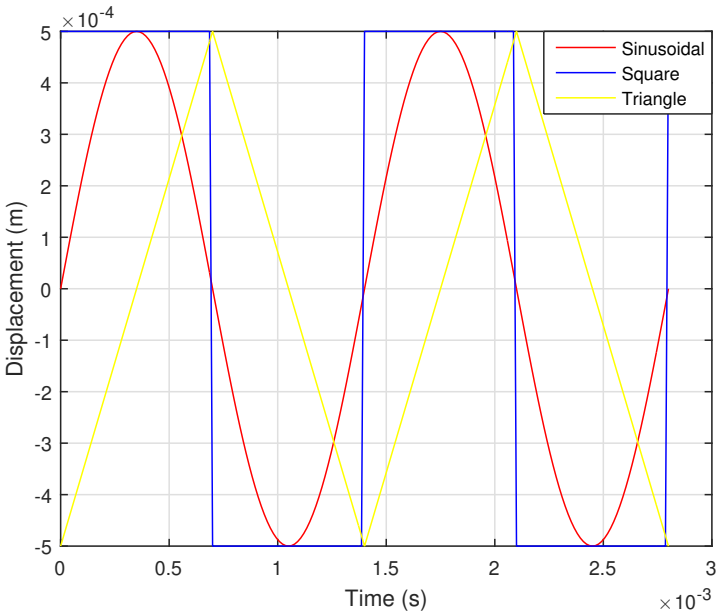

Figure 15 – Sine, triagle, and square waves signals.

after applying sinusoidal, square, and triangular signals to the structure. The inner region of the stress-strain response represents the heat dissipation in a load cycle, and for each signal applied to the structure, different profiles are generated.

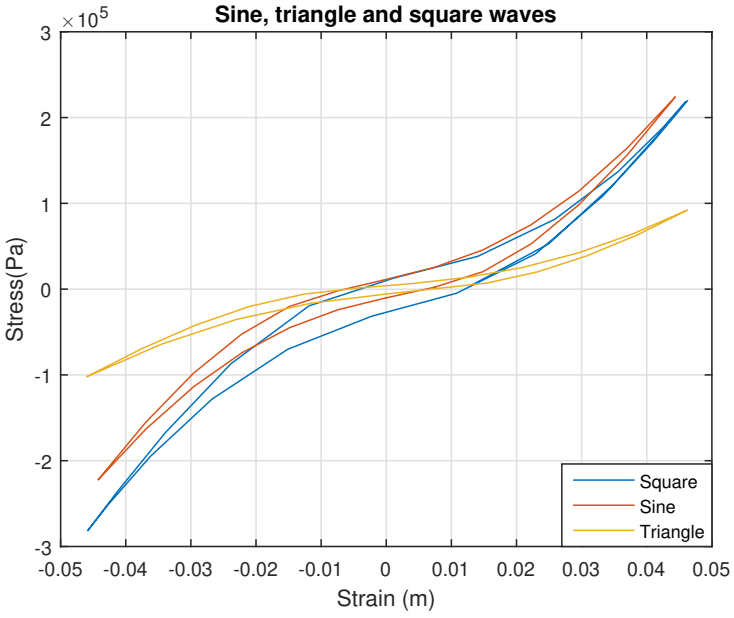

Figure 16 – Hysteresis response after sine, square, and triangle loading cyclic.

3.1.4 Formulation of the Internal Heat Generation

In this step, some parameters, such as the loss modulus and the natural frequencies, must be obtained for the implementation of the equations. Thus, in addition to defining the oscillatory force (Equation 3.1) that will excite the specimen, it is necessary to define

the loss modulus (Equation 3.2), which, unlike the storage modulus (Equation 3.3), which represents the material's ability to store energy elastically and represents the material's ability to dissipate heat through stress ((42, 104–106)).

$$F(t) = A \cdot sin(\omega \cdot t) \tag{3.1}$$

$$E''(\omega, T) = \omega \cdot \int_0^\infty E(t, T) \cdot cos(\omega \cdot t)\, dt \tag{3.2}$$

$$E'(\omega, T) = \omega \cdot \int_0^\infty E(t, T) \cdot sin(\omega \cdot t)\, dt \tag{3.3}$$

where A, ω and, are the amplitude, frequency applied to the specimen and, elasticity modulus, respectively.

As shown at Equation 3.4 ((107)), the complex module is the sum of the storage and loss modules and indicates the relative degree of energy dissipation or damping of the material. Already, Equation 3.5 shows the lag phase (δ) that exists between the curves (stress and strain) ((108)). Figure 17 represents the lag or delay between the stress and strain on viscoelastic materials, which will present this lag variant of 0 until 90 degrees.

$$E^+ = E'(\omega, T) + i \cdot E''(\omega, T) \tag{3.4}$$

$$tg(\delta) = \frac{E''(\omega,T)}{E'(\omega,T)} \tag{3.5}$$

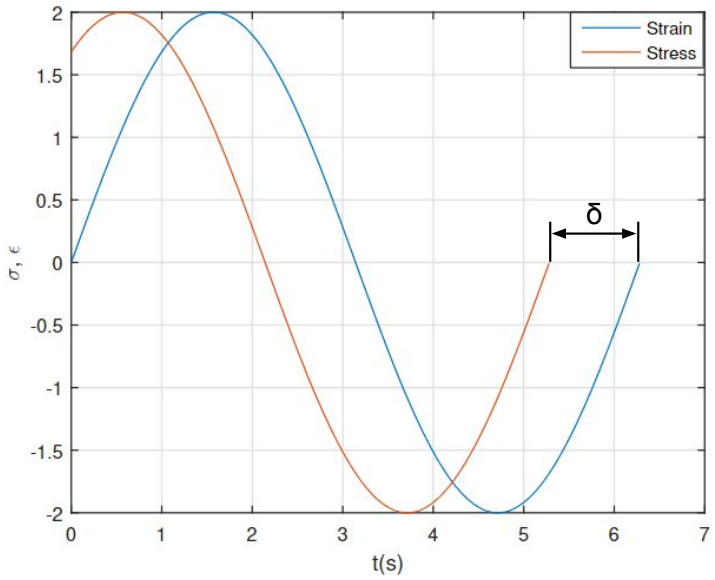

Figure 17 – Example of phase lag.

This made it possible to calculate the dissipated energy and the temperature variation of the specimen per cycle of loading using the Equations 3.6 and 3.7, respectively ((109), (69)).

$$Q_d(t) = \frac{\omega}{2\cdot\pi} \cdot \int_0^{\frac{2\cdot\pi}{\omega}} \sigma(t) \cdot \frac{d\varepsilon(t)}{dt}\, dt \tag{3.6}$$

$$\Delta\dot{T} = \frac{\omega \cdot E''(\omega,t) \cdot \sigma_{max}^2}{\pi \cdot \rho(T) \cdot c(T)} \tag{3.7}$$

According to Equation 3.7, the temperature variation is related to the highest stress encountered per cycle (σ_{max}^2), the loss modulus ($E''(\omega$,t)), and the frequency (ω) applied to the specimen, in addition to the mechanical and thermal properties (ρ, c(T)) of the material. Thus, even if the mechanical and thermal properties, frequency, and loss modulus are the same for the calculation of the temperature variation, the different stresses found in each node of the mesh of the specimen will be responsible for the different temperatures generated. As a result, it is expected that when the specimen is free of internal damage, the temperature distribution should be uniform with no significant temperature variation across the specimen, which should be different when there is damage to the structure.

3.1.5 Determination Experimental of the Mechanical Properties

The use of Equation 3.7 is possible from the determination of some mechanical properties. The specimens used are shown in Figure 18 and follow the ASTM D7028-07 standard. According to Figure 19, loss modulus and storage modulus can be measured for the Prepreg material from the DMA (Dynamic Mechanical Analysis) test, and Figure 20 presents the value for Rohacell Hero 71®. The different equipment used to determine these properties was due to the degradation of the Rohacell Hero 71®, when temperature variation occurred during the DMA test.

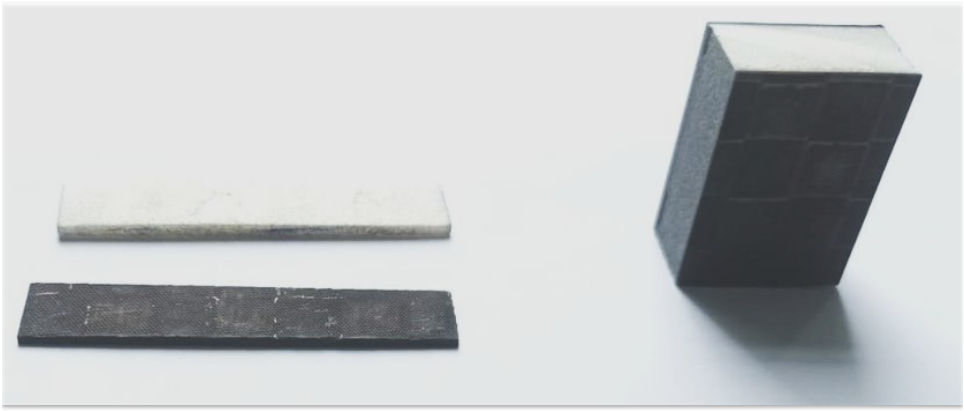

Figure 18 – Specimens (a) DMA test (b) Nanoidentifier.

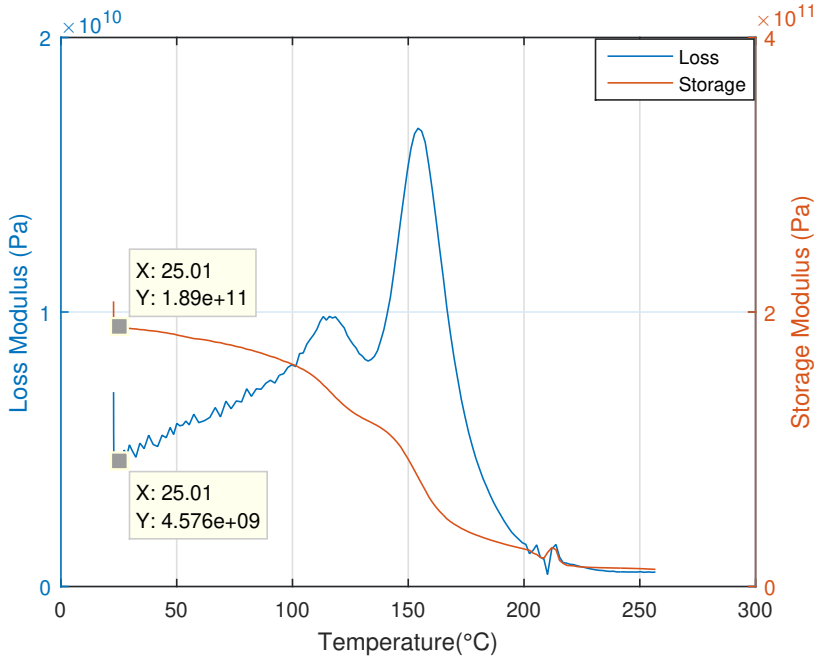

Figure 19 – DMA test to determinate the Loss and Storage Modulus to Prepreg material.

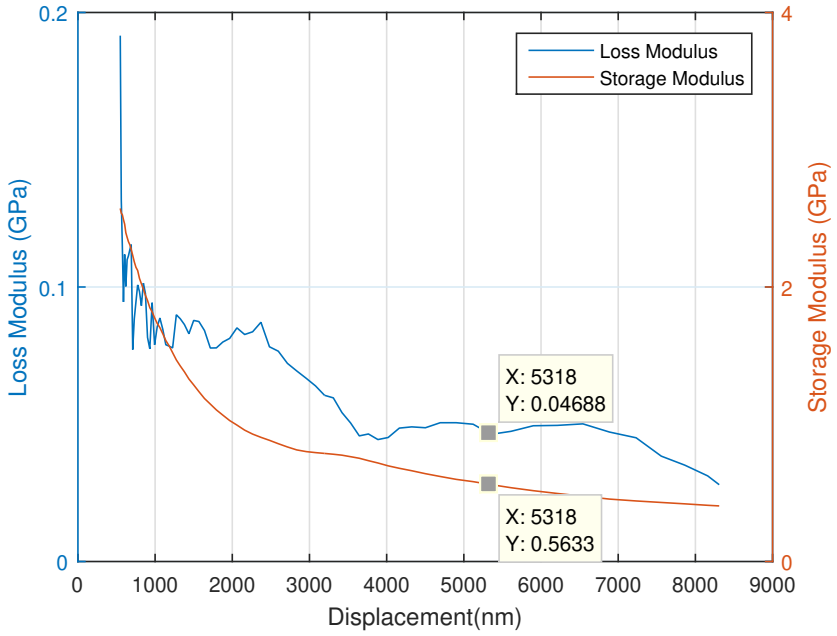

Figure 20 – Identifier test to determinate the Loss and Storage Modulus to Rohacell Hero 71 ®.

3.1.6 Determination Experimental Natural Frequencies from Modal Analysis

Figure 22 and 21 show the equipments used to do the modal test. The impact hammer is used to apply the unit impulse to the composite sandwich beam, which is fixed at one end and has an accelerometer at the other end.

Thus, from these experimental tests, it was possible to obtain the FRF (Function Response Frequency), which allowed finding the natural frequencies of the beam. Together,

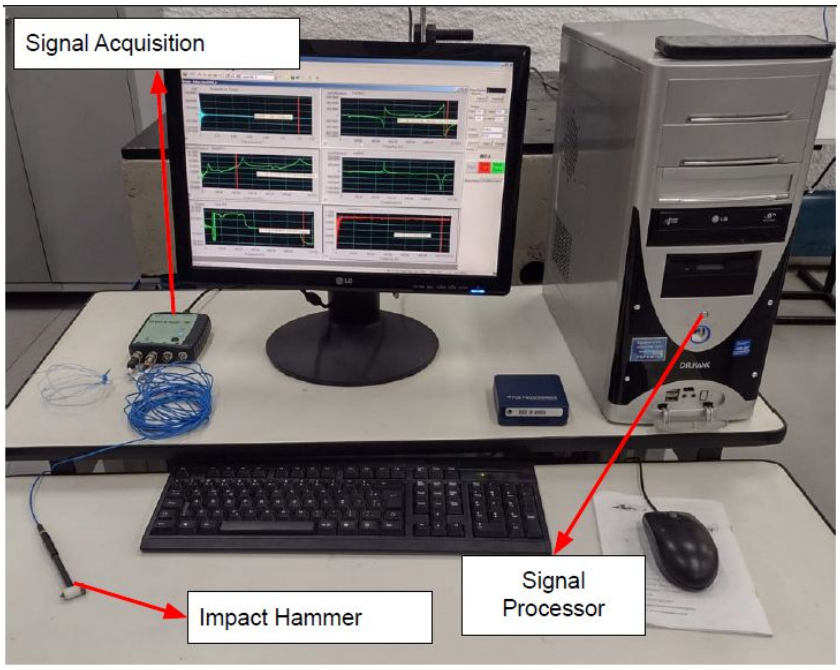

Figure 21 – Acquisition and procession of signals.

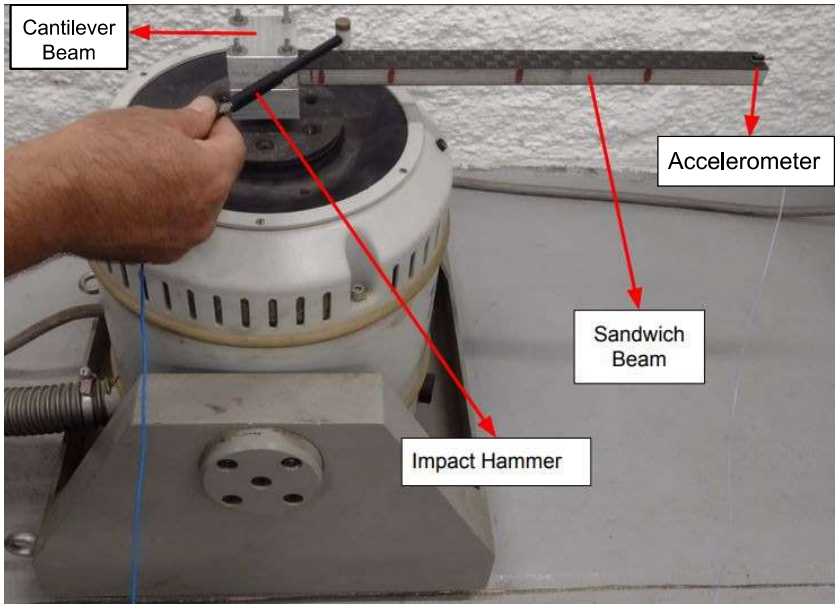

Figure 22 – Equipment to apply the unit impulse in the sandwich beam.

Figure 23 and Figure 24 present conditions that allow to determinate the natural frequencies of the structure, i.e., the phase change of 180° during the test and the changes in the curves imaginary and real to the same frequencies.

Therefore, the comparison between the natural frequencies obtained from numerical analysis and experimental tests can be realized. From the analysis of Table 11, it can be seen that the first, fifth, sixth, and ninth natural frequencies obtained are close, which

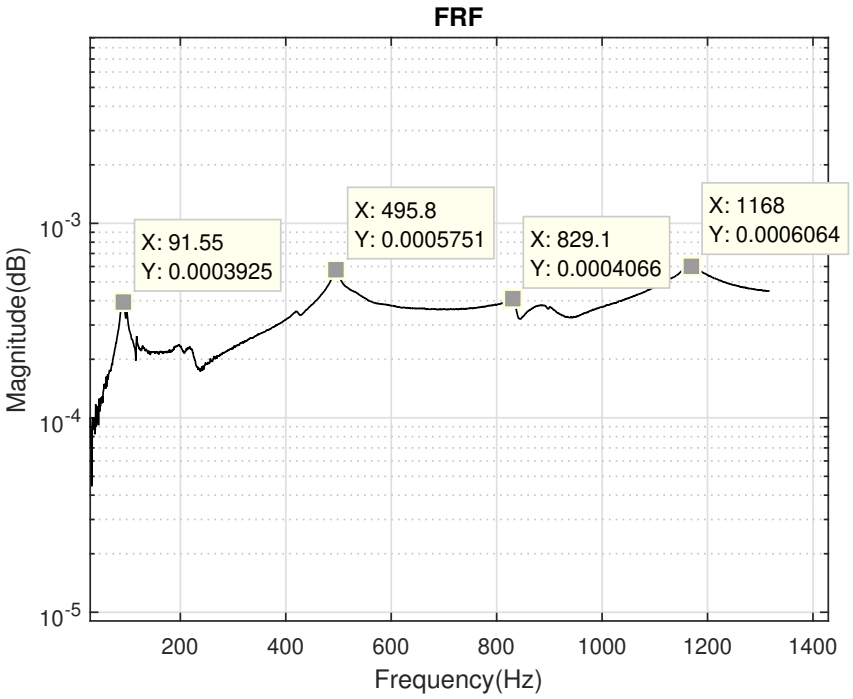

Figure 23 – Experimental Function Frequency Response.

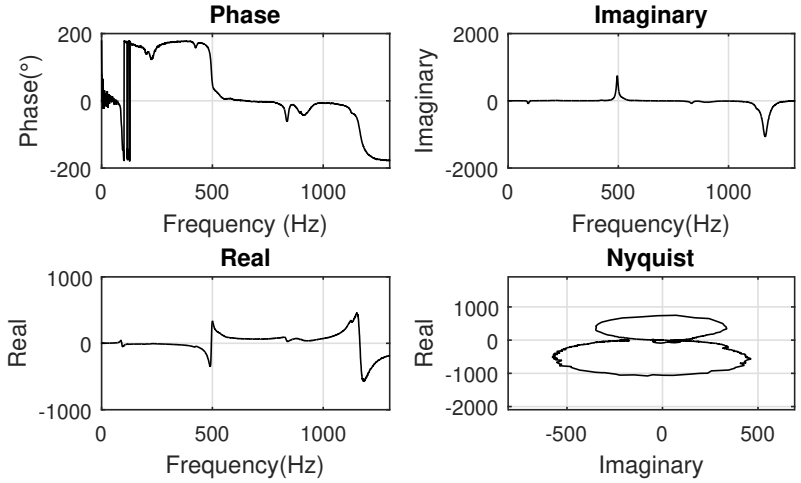

Figure 24 – Response modal analysis.

indicates that the modeling of the structure can represent the real structure. It is interesting to know that the response obtained from numerical analysis permits comparison of the type of mode shape with the frequency found. The other natural frequencies were not obtained due to the positioning chosen by the uniaxial accelerometer, i.e., another way to determine the other natural frequencies, the response in other positioning must be analyzed.

Table 11 – Frequency comparison

Natural Frequency	Experimental	Numerical	Error (%)
ω_{n_1}	91.55	91.48	0.08
ω_{n_2}	-	177.43	-
ω_{n_3}	-	286.46	-
ω_{n_4}	-	296.63	-
ω_{n_5}	495.80	557.72	12.40
ω_{n_6}	829.33	833.56	0.50
ω_{n_7}	-	1006.66	-
ω_{n_8}	-	1023.82	-
ω_{n_9}	1168.00	1151.85	1.38
$\omega_{n_{10}}$	-	1510.78	-

3.2 EXPERIMENTAL ANALYSIS

After the numerical analysis, the experimental analysis was used to expand on the knowledge developed so far, and for this purpose, an experimental setup was created to carry out the tests.

Figure 25 shows the steps proposed for experimental analysis. After the production of specimens and defining the boundary conditions, the frequencies necessary to excite the specimen are obtained. The modeling of the signal of excitation allows the experimental test to be performed, i.e., it is possible to monitor the specimen surface during the tests. The detection or not of the damages will determine if the test must be stopped or not.

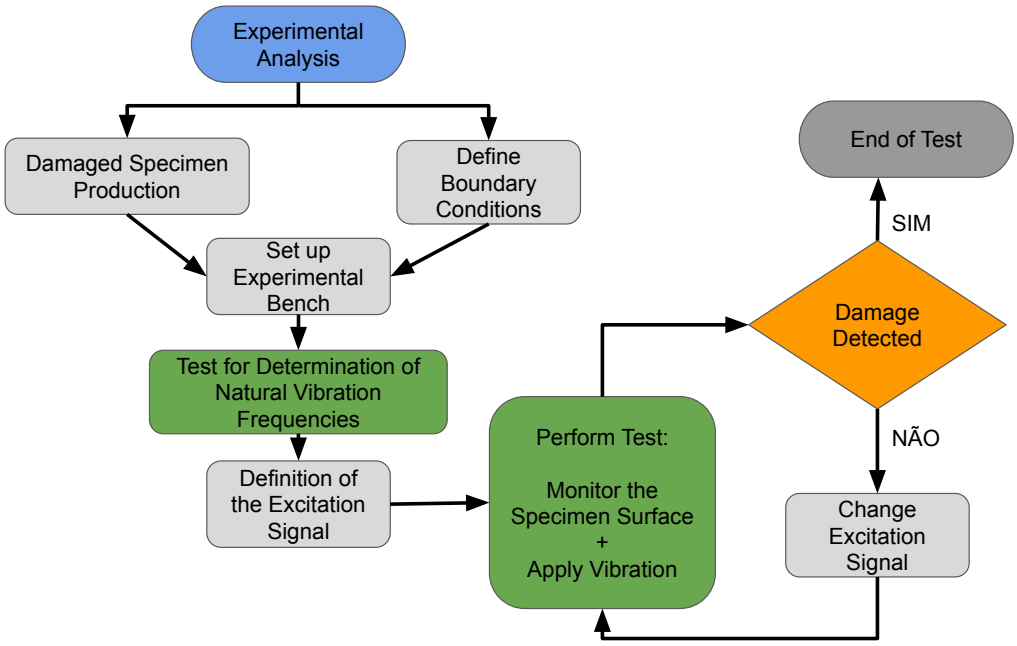

Figure 25 – Methodology used to perform the experimental analysis.

Figure 26 shows first part of the experimental setup; the Specimen is fixed to the metal structure and has a Piezoelectric Actuator attached to it. The Infrared Camera is

positioned to capture the entire surface of the sandwich beam, so that when internal heat is generated, a temperature profile is created on the surface of the material, which can be captured for later analysis.

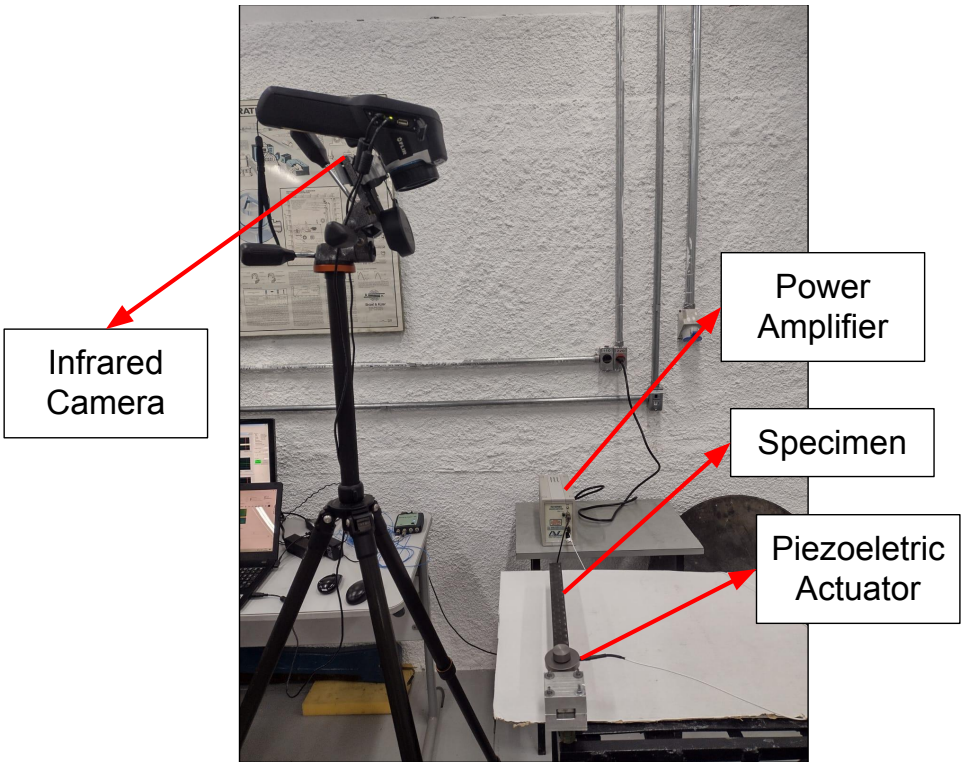

Figure 26 – The first part of the experimental setup for thermal and modal analysis.

Figure 27 shows the second part of the experimental setup: the Signal Control Software sends the signal to the Power Amplifier, which will amplify the signal applied to the Piezoelectric Actuator. The analysis software receives the images from the infrared camera, allowing the captured image to be analyzed.

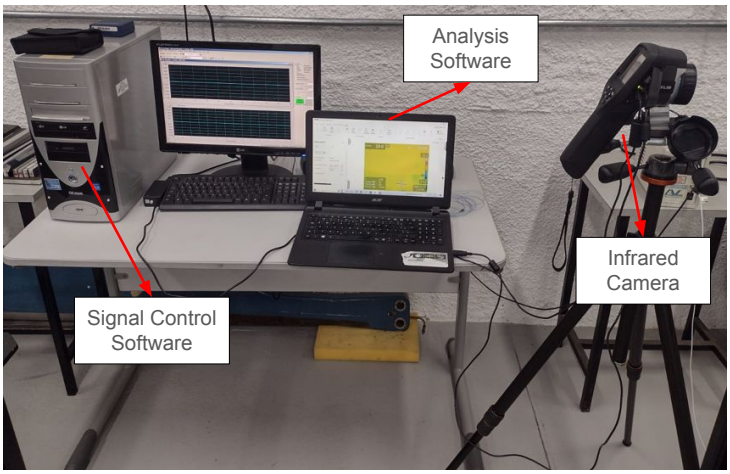

Figure 27 – The second part of the experimental setup for thermal and modal analysis.

The initial analysis was carried out by means of a modal test to determine the new natural frequencies of the system. When the beam was excited by means of a Piezoelectric

Table 12 – New frequencies obtained from the modal test to new configuration.

First (Hz)	Second (Hz)	Third (Hz)	Fourth (Hz)
72.50	179.44	545.65	938.96

Actuator coupled to the structure, the change in the mass of the system required a new test to be carried out. Therefore, to the new configuration, Table 12 show the new values.

To help analyze the temperature profile generated after the experimental test, the displacement of some predetermined points on the beam will be measured. For this purpose, due to the change in the frequency of the excitation signal (obtained from the modal test), some points of the beam are more interesting for analysis.

Of the four new natural frequencies obtained, the first frequency (72.50 Hz) was not used. This choice was made to reduce the number of analyses and because it has a low excitation frequency. Therefore, in order to determine the difference in internal heat generation between the triangular, sinusoidal, and square signals, tests were carried out over a short period of time at the natural frequencies of 179.44, 545.65, and 938.96 Hz and at an arbitrary frequency of 300.00 Hz.

Before starting the experimental tests to analyze the temperature profile on the surface of the material, some interest points to measure the local displacements presented by the beam were determined. To this end, a damaged sandwich beam and an undamaged sandwich beam were used in the tests. The damage is located in the middle of the structure and between the Rohacell and Prepreg materials, as can be seen in Figure 28.

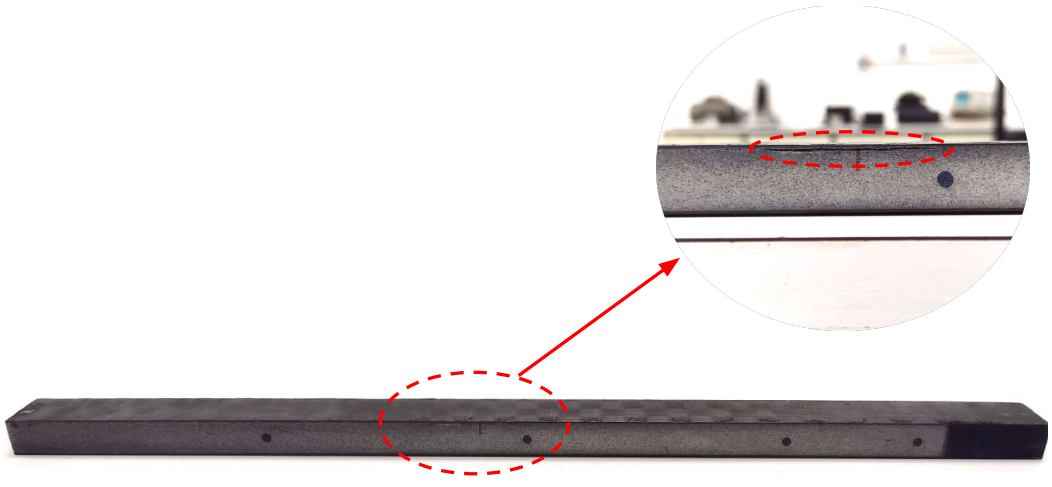

Figure 28 – Sandwich beam damaged.

Knowledge of the vibration nodes is important because they are regions of smaller local displacements and can help determine the shape of the system's modes. Thus, for each natural frequency, the respective vibration nodes generated during excitation are important (Figure 29). In this first analysis, it can be seen that there is no node at a frequency of 179.44 Hz, one node at a frequency of 545.65 Hz, and two nodes at a frequency of 938.96 Hz.

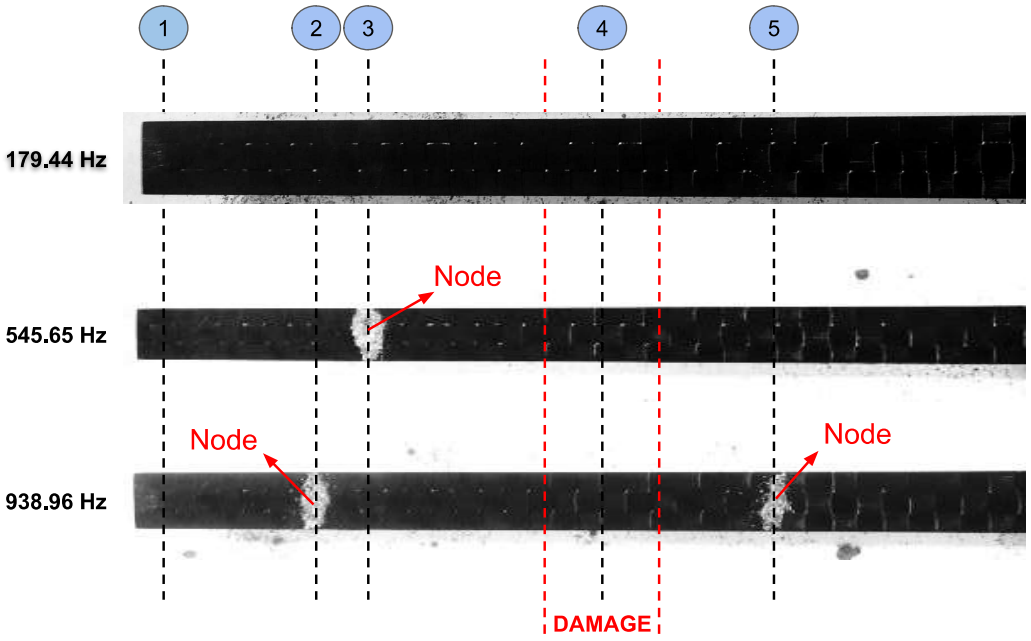

Figure 29 – Identification of vibration nodes using sand during excitation and identification of points of interest for displacement measurements.

Therefore, in addition to the point defined at the free end (number one), the point referring to the damage region (number four) was defined for the position of the node referring to the frequency of 545.65 Hz (number three) and for the nodes referring to the frequency of 938.96 Hz (numbers two and five).

After finding the vibration nodes for each natural frequency and measuring the displacement to each reference point, in order to better explain the setup created to analyze the structures from vibrothermography, Figure 30 shows the region where the infrared camera thermally maps the surface of the material. Due to the presence of the piezoelectric actuator, the region where the actuator is attached to the sample is outside the field of interest.

Figure 30 – Field of interest used in surface mapping.

Therefore, the analysis of the response of the temperature profile on the surface of the material combines three elements: the type of beam (damaged or undamaged), types of signals applied (triangle, sinusoidal, and square), and frequency values (Figure 31).

Thus, capturing the images using the infrared camera will make it possible to analyze the temperature profile generated for each combination involving beam, signal, and

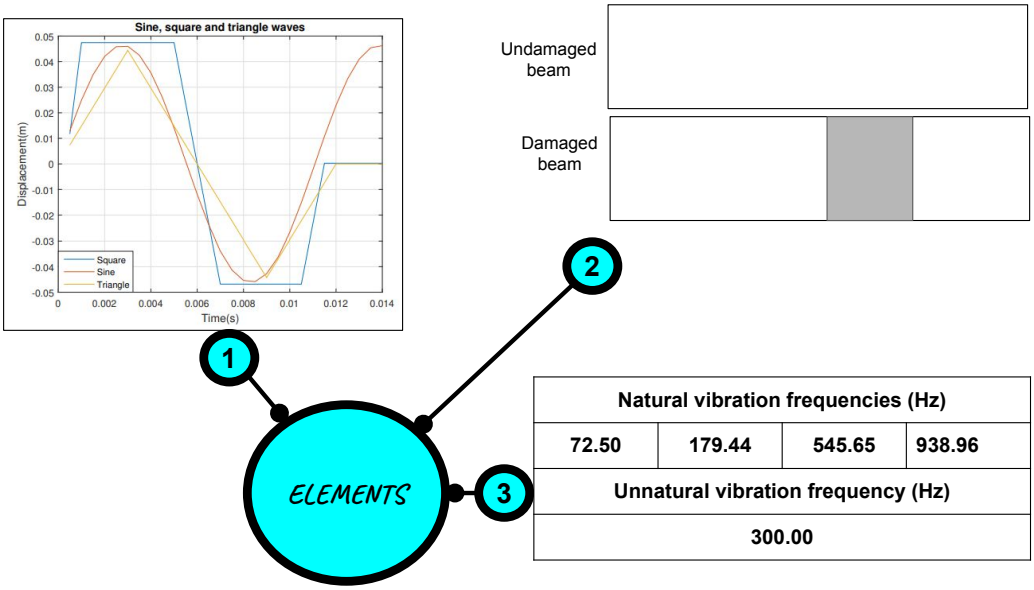

Figure 31 – Combined parameters during experimental tests.

frequency.

4 RESULTS AND DISCUSSION

4.1 NUMERICAL ANALYSIS

After modeling and applying boundary conditions, the sandwich beam was exposed to sine cyclic loading to determine the maximum stress at each node of the discretized beam. According to Figure 32, for an undamaged beam, in the region where the sandwich beam is fixed, the stress profile has its highest value, and from the fixed to the free end, the stresses gradually decrease. Due to the different properties between Rohacell and Prepreg materials, the stress distribution in the structure presents bigger stresses in the skin (Prepreg) in relation to the core (Rohacell).

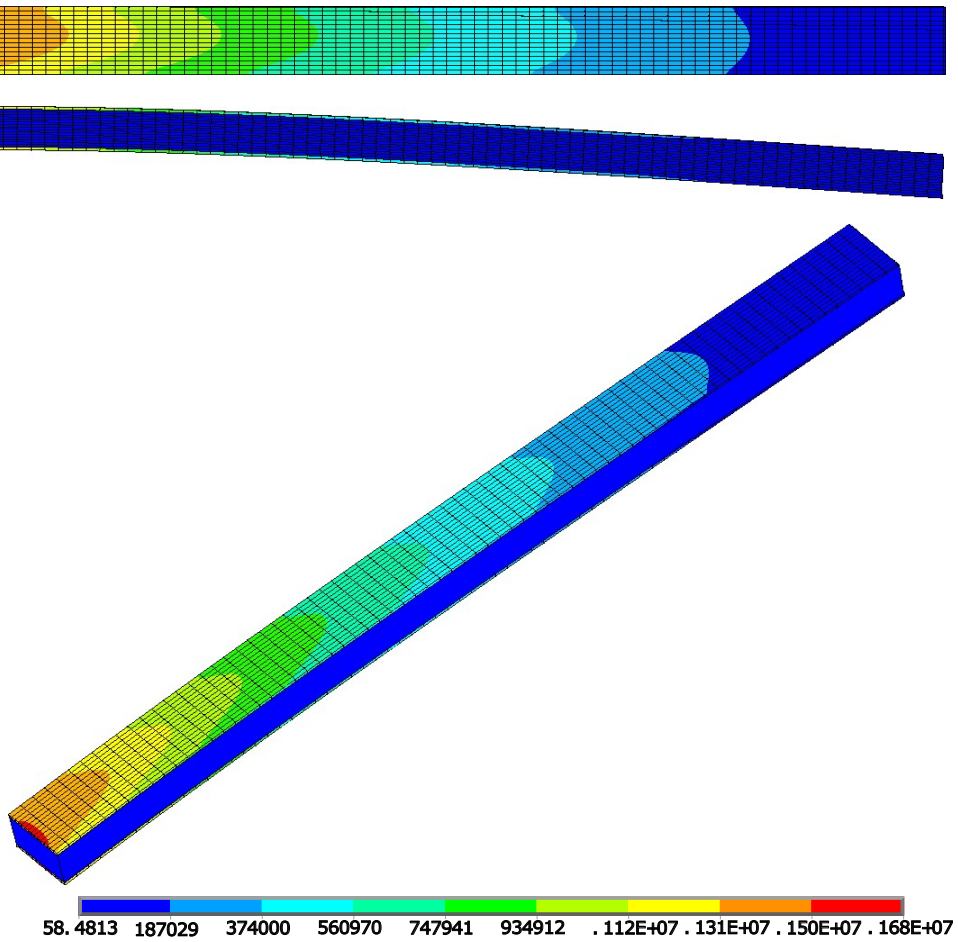

Figure 32 – Stresses generated in the specimen (Pa).

From numerical simulation, in which the stresses are used to calculate the temperature increment per node of the mesh of the structure, it is possible to simulate the response thermal generated on the surface of the structure, as shown in Figure 33.

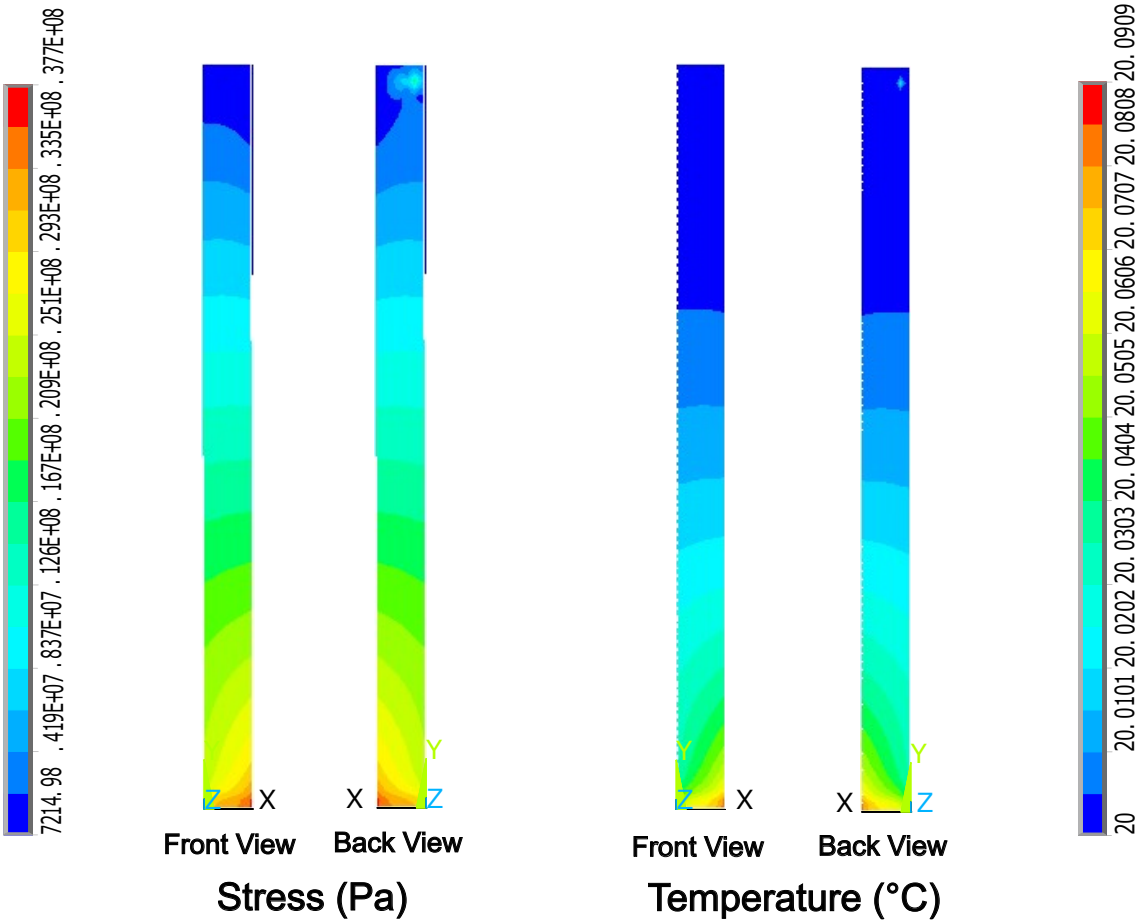

Figure 33 – Temperature and stresses profiles generated in the undamaged beam.

Thus, as described above, it can be seen that there was a higher value near the fixing area and near the area where the force was applied. Therefore, the temperature variation is greater, i.e., the temperature variation is linked to the stress generated. The response of the temperature profile, according to the formulation applied to each node of the discretized structure, can be seen as a gradual decrease from the fixing region.

This result is valid for materials with homogeneous structures (that not present internal damages), i.e., for materials with inhomogeneous structures (that do present internal damages), it is expected that there will be different local property values in the regions with damage, resulting in temperature gradients.

After simulation to determined the profile stresses in the damaged structure, it is possible to relate the stress with the temperature increase at each node of the structure. As shown in Figure 34 and as described throughout the text, the region of the fixed has the highest stress value, which will determine the greatest temperature increase in the structure, and other points that have inhomogeneous local stresses generate different temperature profiles on the surface of the specimen.

Using Equation 3.7, and looking at Figure 34, it can be seen that the calculation of different temperature values for each node of the structure, after the thermal numerical simulation, resulted in a discontinuity of the temperature profile on the surface of the

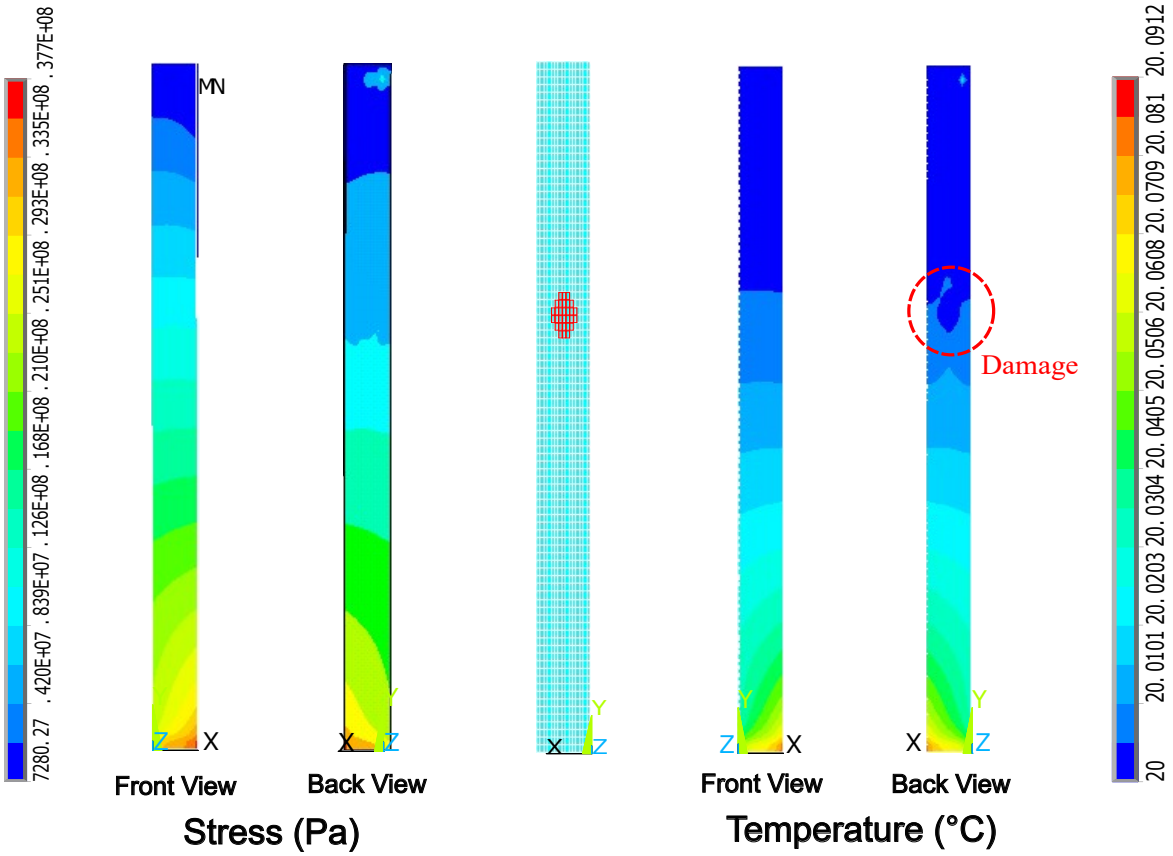

Figure 34 – Temperature and stresses profiles generated in the damaged beam.

specimen, i.e., in the local region where the damage was determined, the modification of the thermal and mechanical properties of the elements resulted in a change in temperature.

On the surface, where the elements were not altered, the temperature profile did not change, but in the region with the damage, the change in the temperature profile indicates the possible presence of damage.

Finally, it can be seen that the temperature gradient generated after the thermal simulation has the same position as the damage induced in the structure. This difference in the temperature profile shows the influence of the viscoelastic characteristics when the structure is cyclically exposed, affirming what was proposed by the formulation presented.

4.2 EXPERIMENTAL ANALYSIS

To improve the analysis of the damaged and undamaged beams, two subsections will be presented. Both analyses will be carried out following the same steps, but the division seeks to better present the analyses.

The analyses carried out from experimental tests had the temperature profile measured in °C and the excitation time of the structure measured in minutes.

4.2.1 Undamaged Beam

The analysis of the undamaged beam can be classified in two topics, with or without the use of natural frequencies, so that a later comparison between the responses is possible.

Before analyzing the temperature profile generated on the surface of the structure, the displacements of the beam for the arbitrary frequency of 300.00 Hz and for each natural frequency were measured following some points of interest: nodes, anti-nodes, and free ends (according to Figure 29). Because the frequencies of 179.44 and 300.00 Hz don't have nodes during excitation, only three points were chosen to represent the displacements of the beam. When excite at frequencies of 545.65 or 938.96 Hz, there are nodes and antinodes present during the excitation, which required more points of measurements of the displacements.

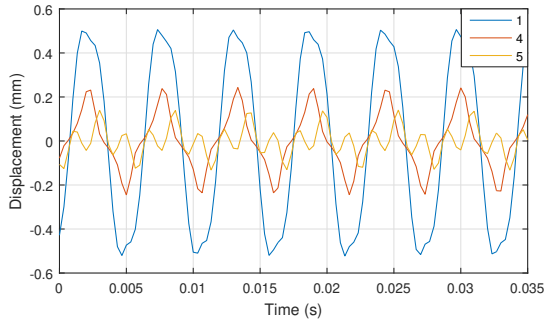

(a) 179.44 Hz

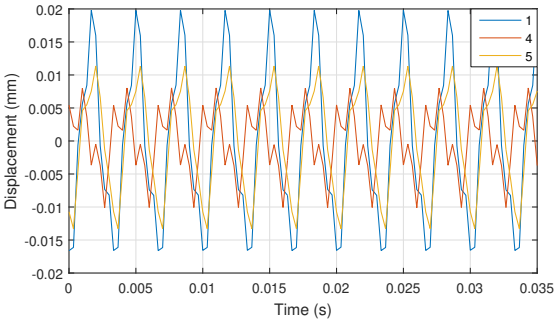

(b) 300.00 Hz

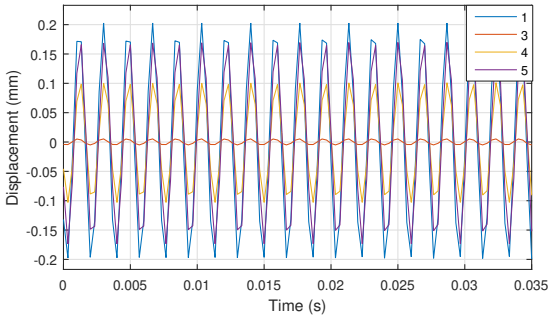

(c) 545.65 Hz

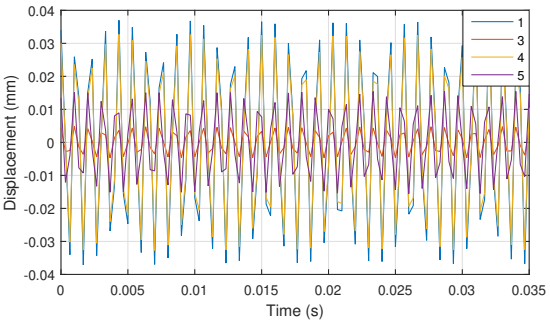

(d) 938.96 Hz

Figure 35 – Displacements reference points.

Considering the excitation from the sinusoidal signal, Figure 35 shows the displacement measurements for each reference point, and these responses will be used in the final analysis. It is interesting to note that for all frequencies, reference point number one had a bigger displacement, and reference points located in the nodal region presented a smaller displacement.

To find out if the results shown in Figure 36 are correct, i.e., if they will be repeated on other specimens, two other specimens are shown in Appendix C. The response analyses for sinusoidal, square, and triangular signals at frequencies of 179.44, 545.65, and 938.36 Hz show the same characteristics.

Already to analyze the temperature profile generated on the surface of the material after mechanical excitation, Figure 36 has the results.

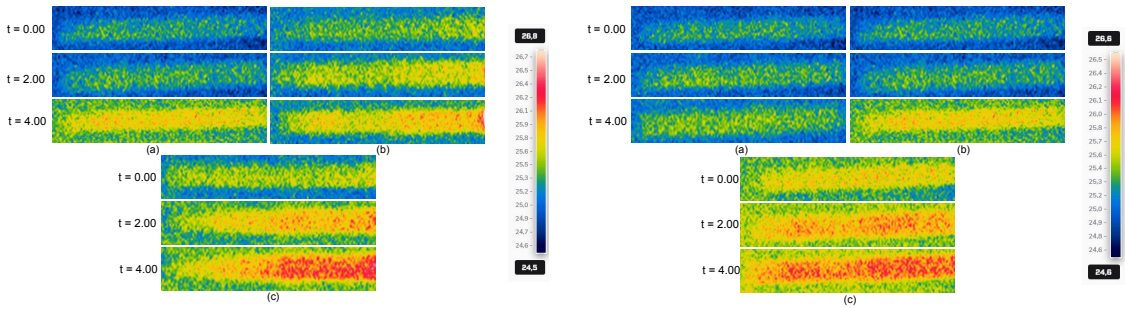

(I) 179.44 Hz

(II) 300.00 Hz

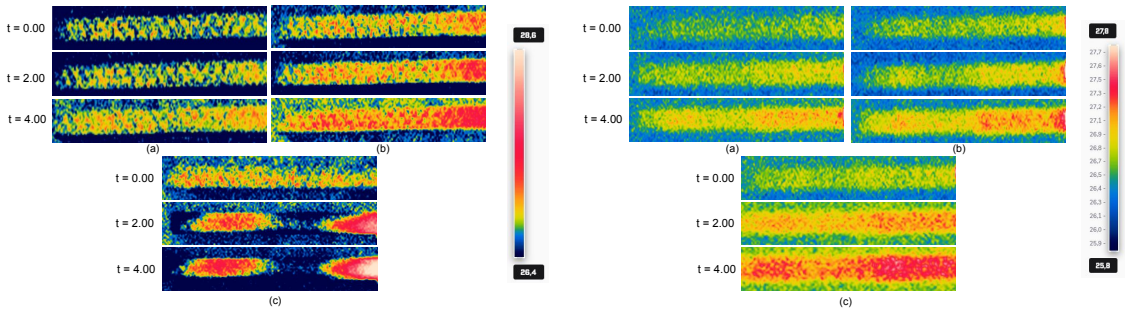

(III) 545.65 Hz

(IV) 938.96 Hz

Figure 36 – Temperature profile for an undamaged sandwich beam. In I), II), III), and IV), there is: a) a triangular wave; b) a sine wave; c) a square wave.

Figure 36 shows the response after excitation using triangular, sine, and square waves for the frequencies defined during the experimental tests. In all tests, i.e., for all frequencies, the temperature profile along the beam captured by the infrared camera increased. For the square wave at a frequency of 545.65 Hz, the temperature profile behaved differently from the other frequencies: the temperature in the middle of the beam, i.e., at the location of point four, was lower.

At a frequency of 179.44 Hz, the response of the temperature profile was similar to that of the profile generated at a frequency of 300.00 Hz, i.e. the temperature gradient decreased from the fixing region to the free end.

It can therefore be seen that, of the three signals used to excite the structure, the triangular signal generated the least variation in the temperature profile, i.e., the least was the excitation induced by the triangle wave during these four minutes. The square signal, on the other hand, had a greater variation in the temperature profile, i.e., this signal induces greater internal heat generation on the structure.

4.2.2 Damaged Beam

In this new step of analysis, new considerations must be presented. Because the frequency of 300.00 Hz did not show characteristics that could improve damage detection, this frequency was taken out of the analysis. Natural frequencies with values of 179.44, 545.65, and 938.96 Hz and the excitation time of the structure of four minutes were used again.

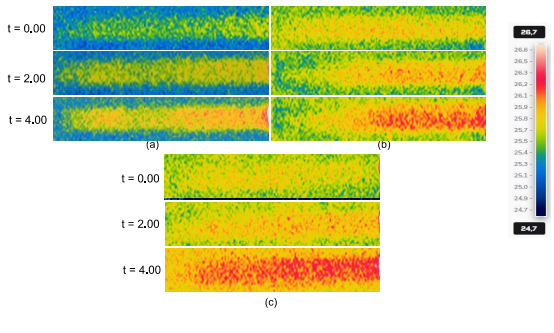

(a) 179.44 Hz

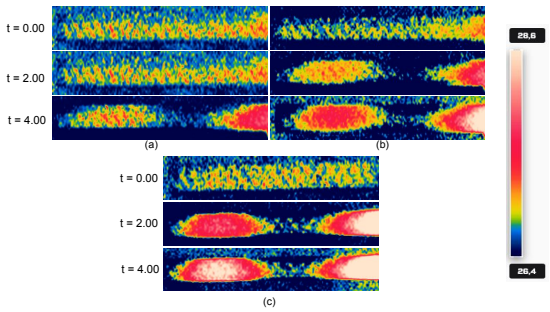

(b) 545.65 Hz

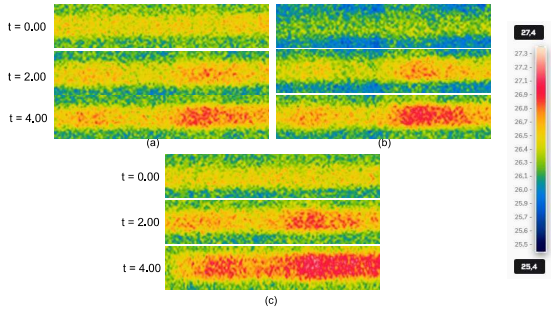

(c) 938.96 Hz

Figure 37 – Temperature profile for an undamaged sandwich beam. In I), II), and III), there is: a) a triangular wave; b) a sine wave; c) a square wave.

From Figure 37 the new characteristics to frequency of the 545.65 Hz were obtained. According to what was presented for the damaged beams and different from what was obtained for the undamaged beam, a pattern showing regions with lower and higher temperature gradients was found on the surface of the structure for the three types of signals used, i.e., in the region of localization of the damage, the similar characteristics were found to time of four minutes.

Experimental tests have shown that the excitation of the structure results in the generation of internal heat, which alters the surface temperature profile according to the excitation time. It is also known that when the structure shows internal damage, the local generation of internal heat is altered, i.e., the local temperature on the surface of the material will show temperature gradients that demonstrate the presence of damage.

4.2.3 Comparison Between the Thermal Responses of the Undamaged and Damaged Beams

In this section, reference point 4 was established at a distance x from the start of the mapping area provided by the infrared camera, in order to map the local acceleration in the damage region, and subsequently calculate the respective local displacement of the beam.

Figure 38 shows the thermograms for the 179.44 Hz frequency, which have a greater temperature increase for the damaged beam after four minutes. The displacement measurements for point four for both beams show close values, and the thermogram response shows similar characteristics. In this case, the excitation used did not make it possible to detect a significant change in the temperature profile on the surface of the beam.

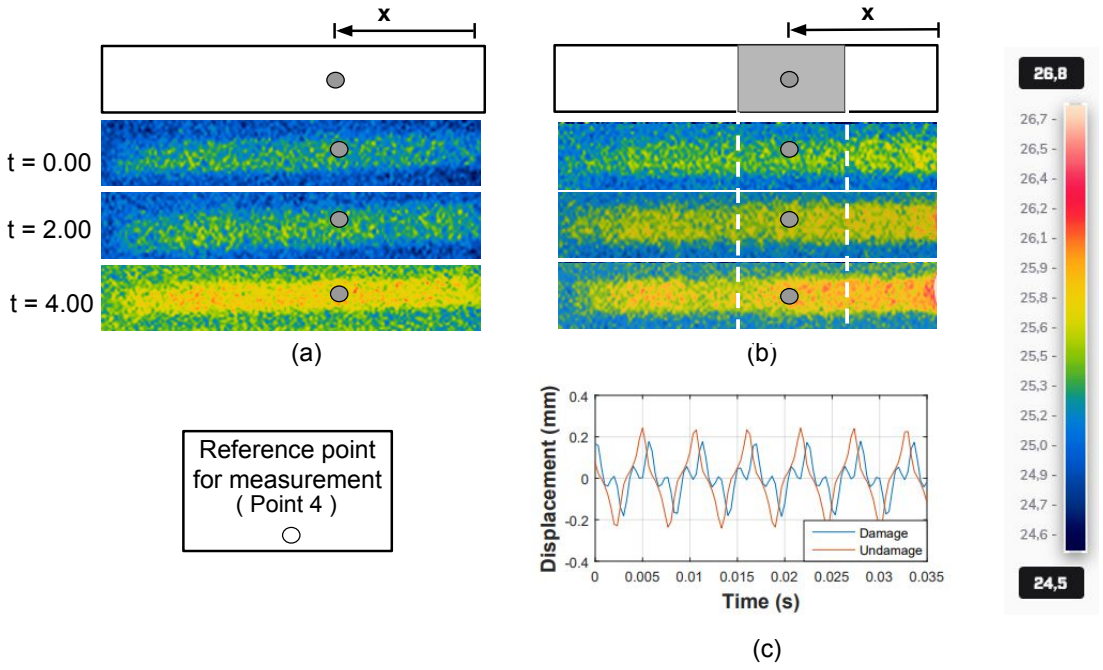

Figure 38 – Sinusoidal response at a frequency of 179.44 Hz: a) Undamaged Beam, b) Damage Beam, c) Displacements to point four.

In the case of Figure 39, to frequency of the 545.65 Hz, to the thermograms captured in the undamaged beam (Figure 39 (a)), an increase in temperature was observed throughout the beam, unlike what was found for the damaged beam (Figure 39 (b)), in which, at times 2 and 4 minutes, a different temperature profile was observed in the region of the damage, with a lower temperature measured by the infrared camera. When analyzing the displacements measured for points 4 initially defined in the damaged and undamaged beams as a reference (Figure 39 (c)), an oscillation three times greater was observed for the damaged beam compared to the undamaged beam.

Just as it was presented for the 179.44 Hz frequency, the displacements measurements to the point four in damaged and undamaged beams are close value, but when the analyse

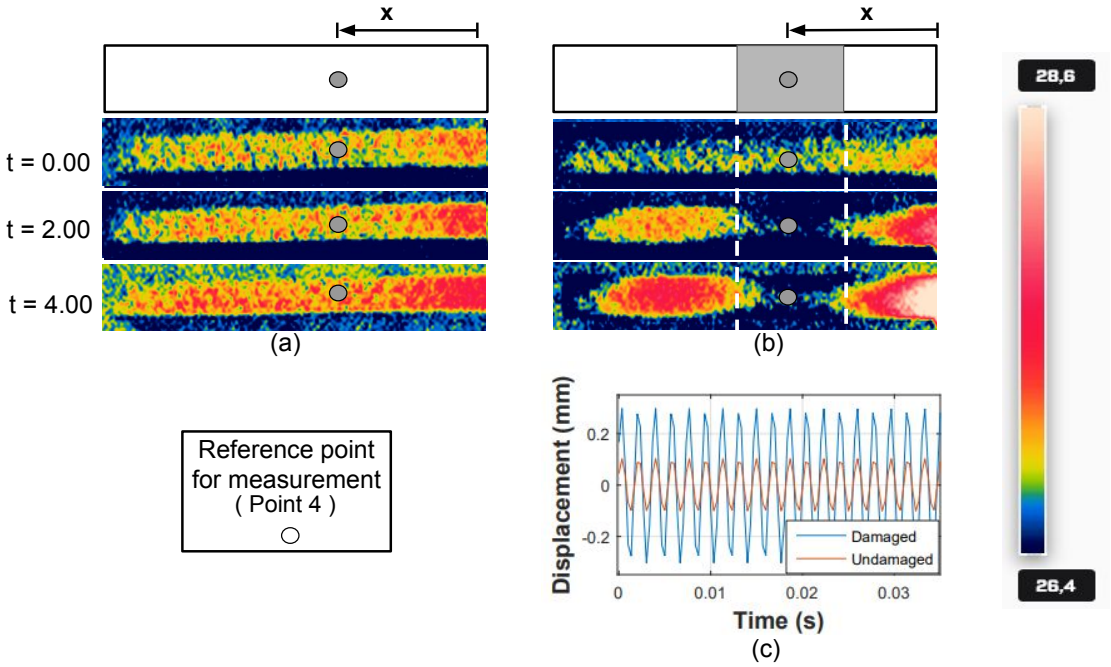

Figure 39 – Sinusoidal response at a frequency of 545.65 Hz: a) Undamaged Beam, b) Damage Beam, c) Displacements to point four.

is did about the thermograms, it is possible to note that in the region of the damage occured an bigger temperature variation , what can be may be due to the generation of internal heat in the region of the damage.

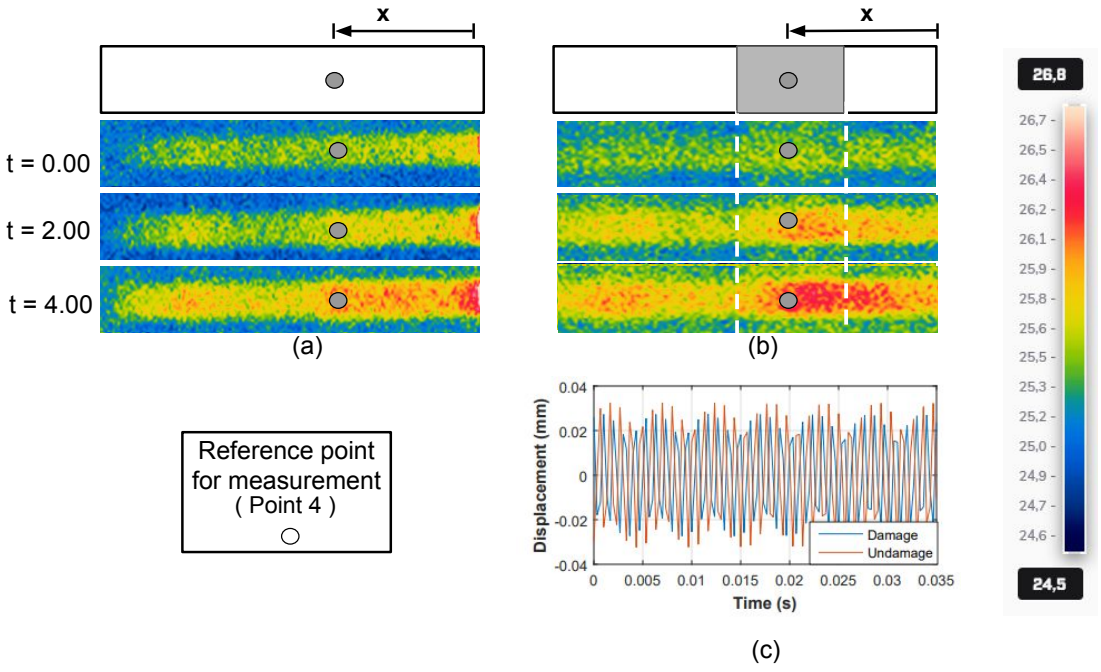

Figure 40 – Sinusoidal response at a frequency of 939.96 Hz: a) Undamaged Beam, b) Damage Beam,
c) Displacements to point four.

5 CONCLUSION AND FUTURE WORK

5.1 CONCLUSION

Damage detection is essential to ensuring the safe use of equipment and structures. Vibrothermography is a good active detection technique and can use the characteristics of vibration systems to improve damage detection. Among the heat generation mechanisms shown in the studies presented in Section 2.2, this work initially applies a formulation that considers the viscoelastic phenomenon.

According to the numerical simulation, some regions showed greater local variation in the surface temperature profile, i.e., in the region where the local stresses had greater variation, as can be seen in the region where the cyclic stress was applied and in the region where the beam was fixed, this characteristic was present. Therefore, following this method of analysis, in which a formulation is available to calculate the temperature increment per node of the mesh defined for the structure, which considers viscoelastic properties, it was possible to conclude that viscoelasticity is present in composite materials, but it must be analyzed with the implementation of the other characteristics of the system, such as heat transfer and improvement of displacement measurements at natural frequencies.

In the initial response of the experiments, the square, sine, and triangular signals had different responses, i.e., the square signal generated more internal heat when analyzed for the same excitation time, and the triangular signal generated less internal heat. The square signal imposes a longer exposure time for the specimen under maximum stress, while the triangular and sinusoidal signals reach maximum stress in a minimum amount of time.

Considering the temperature profile generate on the surface of the material, the result can have some contributes, how the viscoelstic response of the material (which (lag between stress and displacement), energy generation due the local deformation along of the beam, and the heat transfer between the beam and the environment.

From analyses of the damage region, where the displacement change with the natural frequency used during the excitation of the structure, to the frequencies which the displacements are bigger, the heat transfer between beam and the environment is bigger too, what result in a smaller temperature in the region of damage. Already to the frequencies which the displacements are smaller, both the energy generated by deformation and the energy generated due to the viscoelastic response of the material are greater than the energy exchanged with the environment, which results in an increase in local temperature.

Thus, in the region of the damage, for frequency of 545.65 Hz, where the damage is away from the vibration node, the temperatures are smaller, and for frequency of 938.96

Hz, where the damage is near the vibration node, the temperature is bigger in relation to the temperature in other regions of the beam. In the free end, where the displacement is larger than all analyses, the temperature is smaller, i.e., the energy lost to the environment is bigger when compared with the sum of the energy generated by viscoelastic behavior with the energy generated by deformation of the beam.

5.2 FUTURE WORK:

Some suggestions for future work can be suggested as a continuation of this doctoral dissertation:

Numerical analysis from the proposed code:

- Implement heat exchange between the beam and the environment;
- Apply a multi-harmonic signal to the simulations;
- Simulate other types of damage, such as porosity and cracks.

Experimental tests:

- Combine the vibrothermography technique with another active detection technique, such as pulsed thermography or long-pulse thermography.

Post-processing:

- Use post-processing techniques such as algorithms, statistical methods, etc.

BIBLIOGRAPHY

1 CIAMPA, F. et al. Recent advances in active infrared thermography for non-destructive testing of aerospace components. *Sensors*, MDPI, v. 18, n. 2, p. 609, 2018. Citado 4 vezes nas páginas 1, 2, 12, and 14.

2 ZAMAN, A.; GUTUB, S. A.; WAFA, M. A. A review on frp composites applications and durability concerns in the construction sector. *Journal of Reinforced Plastics and Composites*, SAGE Publications Sage UK: London, England, v. 32, n. 24, p. 1966–1988, 2013. Citado na página 1.

3 MCILHAGGER, A.; ARCHER, E.; MCILHAGGER, R. 3 manufacturing processes for composite materials and components for aerospace applications. In: IRVING, P.; SOUTIS, C. (Ed.). *Polymer Composites in the Aerospace Industry*. [S.l.: s.n.], 2015. Citado na página 1.

4 VELASCO-PARRA, J. A.; RAMON-VALENCIA, B. A.; MORA-ESPINOSA, W. J. Composite materials reinforced with ceramic waste and matrix of unsaturated polyester for applications in the automotive industry. *DYNA*, scieloco, v. 87, p. 251 – 258, 03 2020. ISSN 0012-7353. Citado na página 1.

5 BAGAVATHIAPPAN, S. et al. Infrared thermography for condition monitoring–a review. *Infrared Physics & Technology*, Elsevier, v. 60, p. 35–55, 2013. Citado na página 1.

6 USAMENTIAGA, R. et al. Infrared thermography for temperature measurement and non-destructive testing. *Sensors*, Multidisciplinary Digital Publishing Institute, v. 14, n. 7, p. 12305–12348, 2014. Citado na página 1.

7 STALMACH, O. et al. Contribution to the determination of the thermal emissivity of the composite material using longwave infrared camera. *MATEC Web Conf.*, v. 244, p. 01026, 2018. Citado na página 1.

8 STINCHCOMB, W. W. et al. *Mechanics of Nondestructive Testing*. [S.l.: s.n.], 1980. Citado 2 vezes nas páginas 1 and 7.

9 RUSSELL, S. S. *An investigation of the excitation frequency dependent behavior of fiber reinforced epoxy composites during vibrothermographic inspection*. [S.l.: s.n.], 1982. Citado na página 1.

10 HARIZI, W. et al. Mechanical damage assessment of glass fiber-reinforced polymer composites using passive infrared thermography. *Composites Part B: Engineering*, Elsevier, v. 59, p. 74–79, 2014. Citado na página 1.

11 HARIZI, W. et al. Mechanical damage assessment of polymer–matrix composites using active infrared thermography. *Composites Part B: Engineering*, Elsevier, v. 66, p. 204–209, 2014. Citado na página 1.

12 SENTHILKUMAR, M.; SREEKANTH, T.; REDDY, S. M. Nondestructive health monitoring techniques for composite materials: A review. *Polymers and Polymer Composites*, SAGE Publications Sage UK: London, England, v. 29, n. 5, p. 528–540, 2021. Citado na página 1.

13 RAMZAN, B. et al. Pixel frequency based railroad surface flaw detection using active infrared thermography for structural health monitoring. *Case Studies in Thermal Engineering*, Elsevier, v. 27, p. 101234, 2021. Citado na página 1.

14 MüLLER, J. P.; DELL'AVVOCATO, G.; KRANKENHAGEN, R. Assessing overload-induced delaminations in glass fiber reinforced polymers by its geometry and thermal resistance. *NDT & E International*, v. 116, p. 102309, 2020. ISSN 0963-8695. Citado na página 1.

15 VAVILOV, V. P.; BURLEIGH, D. D. Review of pulsed thermal ndt: Physical principles, theory and data processing. *NDT & E International*, v. 73, p. 28–52, 2015. ISSN 0963-8695. Citado na página 1.

16 RYU, S. Damage detection of composite materials via electrical resistance measurement and ir thermography: A review. Engineering Archive, 2021. Citado na página 1.

17 NGAONGAM, C.; EKPANYAPONG, M.; UJJIN, R. Surface crack detection by using vibrothermography technique. *Quantitative InfraRed Thermography Journal*, Taylor & Francis, v. 0, n. 0, p. 1–12, 2022. Citado na página 2.

18 GUO, X.; ZHU, L. Vibro-thermography of calibrated defects in hybrid plates focusing on viscoelastic heat generation. *Quantitative InfraRed Thermography Journal*, Taylor & Francis, v. 18, n. 5, p. 314–331, 2021. Citado na página 2.

19 LI, Y. et al. Investigation into vibration characteristic in vibrothermography. *Photonic Sensors*, Springer, v. 9, n. 2, p. 108–114, 2019. Citado na página 2.

20 MABROUKI, F. et al. Numerical modeling of vibrothermography based on plastic deformation. *NDT & E International*, Elsevier, v. 43, n. 6, p. 476–483, 2010. Citado na página 2.

21 MIN, Q.-x. et al. Study on optimization method of test conditions for fatigue of engineering crack detection using lock-in vibrothermography. *Infrared Physics & Technology*, Elsevier, v. 83, p. 17–23, 2017. Citado na página 2.

22 HOLLAND, S. D. Thermographic signal reconstruction for vibrothermography. *Infrared Physics & Technology*, Elsevier, v. 54, n. 6, p. 503–511, 2011. Citado na página 2.

23 RENSHAW, J. et al. Vibration-induced tribological damage to fracture surfaces via vibrothermography. *International Journal of Fatigue*, Elsevier, v. 33, n. 7, p. 849–857, 2011. Citado na página 2.

24 XU, C. et al. Experimental investigation on the detection of multiple surface cracks using vibrothermography with a low-power piezoceramic actuator. *Sensors*, MDPI, v. 17, n. 12, p. 2705, 2017. Citado na página 2.

25 VADDI, J. S.; HOLLAND, S. D.; KESSLER, M. R. Absorptive viscoelastic coatings for full field vibration coverage measurement in vibrothermography. *NDT & E International*, Elsevier, v. 82, p. 56–61, 2016. Citado na página 2.

26 BHARGAVA, V.; ABU-NABAH, B. A.; ALKHADER, M. A theoretical approach towards the modeling of vibrothermography using finite element methods. *European Journal of Mechanics, A Solids*, Elsevier, v. 91, p. 104389, 2022. Citado na página 2.

27 HENNEKE, I. et al. *Vibrothermography: Investigation, development, and application of a new nondestructive evaluation technique*. [S.l.], 1986. Citado na página 2.

28 HENNEKE, E. G. Vibrothermography applied to polymer matrix composites. In: _____. *Manual on Experimental Methods for Mechanical Testing of Composites*. Dordrecht: Springer Netherlands, 1989. p. 129–137. Citado na página 3.

29 POTET, P.; LESBRE, F.; BATHIAS, C. Quantitative characterization of impact damage in composite materials—a comparison between computerized vibrothermography and x-ray tomography. *Nondestructive Testing and Evaluation for Manufacturing and Construction; dos Reis, HLM, Ed*, p. 95–105, 1989. Citado na página 3.

30 SEIFOORI, S. et al. An experimental study on damage intensity in composite plates subjected to low-velocity impacts. *Polymer Testing*, v. 93, p. 106887, 2021. ISSN 0142-9418. Citado 3 vezes nas páginas 6, 11, and 16.

31 KATUNIN, A.; WRONKOWICZ-KATUNIN, A.; WACHLA, D. Impact damage assessment in polymer matrix composites using self-heating based vibrothermography. *Composite Structures*, v. 214, p. 214–226, 2019. ISSN 0263-8223. Citado 4 vezes nas páginas 6, 9, 11, and 23.

32 PIECZONKA, L. et al. Modelling and numerical simulations of vibrothermography for impact damage detection in composites structures. *Structural Control and Health Monitoring*, v. 20, p. 626–638, 04 2013. Citado 2 vezes nas páginas 6 and 11.

33 XU, J. et al. Terahertz imaging and vibro-thermography for impact response in carbon fiber reinforced plastics. *Infrared Physics & Technology*, v. 109, p. 103413, 2020. ISSN 1350-4495. Citado 3 vezes nas páginas 6, 16, and 18.

34 GAUDENZI, P. et al. On the evaluation of impact damage on composite materials by comparing different ndi techniques. *Composite Structures*, v. 118, p. 257–266, 2014. ISSN 0263-8223. Citado 3 vezes nas páginas 6, 11, and 16.

35 SEIFOORI, S.; IZADI, R.; YAZDINEZHAD, A. Impact damage detection for small- and large-mass impact on cfrp and gfrp composite laminate with different striker geometry using experimental, analytical and fe methods. *Acta Mechanica*, v. 230, 12 2019. Citado 3 vezes nas páginas 6, 12, and 16.

36 SEGERS, J. et al. In-plane local defect resonances for efficient vibrothermography of impacted carbon fiber-reinforced polymers (cfrp). *NDT & E International*, v. 102, p. 218–225, 2019. ISSN 0963-8695. Citado na página 6.

37 HEDAYATRASA, S. et al. Vibro-thermal wave radar: Application of barker coded amplitude modulation for enhanced low-power vibrothermographic inspection of composites. *Materials*, v. 14, n. 9, 2021. ISSN 1996-1944. Citado 4 vezes nas páginas 6, 11, 12, and 16.

38 VAVILOV, V.; ŚWIDERSKI, W.; DERUSOVA, D. Ultrasonic and optical stimulation in ir thermographic ndt of impact damage in carbon composites. *Quantitative InfraRed Thermography Journal*, Taylor & Francis, v. 12, n. 2, p. 162–172, 2015. Citado na página 6.

39 HEDAYATRASA, S. et al. Vibrothermographic spectroscopy with thermal latency compensation for effective identification of local defect resonance frequencies of a cfrp with bvid. *NDT & E International*, v. 109, p. 102179, 10 2019. Citado na página 6.

40 HE, Y. et al. Shared excitation based nonlinear ultrasound and vibrothermography testing for cfrp barely visible impact damage inspection. *IEEE Transactions on Industrial Informatics*, IEEE, v. 14, n. 12, p. 5575–5584, 2018. Citado na página 6.

41 FERNANDES, H. et al. Thermographic non-destructive evaluation of carbon fiber-reinforced polymer plates after tensile testing. *Journal of Nondestructive Evaluation*, Springer, v. 34, n. 4, p. 1–10, 2015. Citado 2 vezes nas páginas 7 and 11.

42 KATUNIN, A. Criticality of the self-heating effect in polymers and polymer matrix composites during fatigue, and their application in non-destructive testing. *Polymers*, v. 11, p. 19, 01 2019. Citado 2 vezes nas páginas 7 and 26.

43 KATUNIN, A.; WACHLA, D. Analysis of defect detectability in polymeric composites using self-heating based vibrothermography. *Composite Structures*, v. 201, p. 760–765, 2018. ISSN 0263-8223. Citado 4 vezes nas páginas 7, 9, 11, and 16.

44 ZHANG, H. et al. Comparative study on submillimeter flaws in stitched t-joint carbon fiber reinforced polymer by infrared thermography, microcomputed tomography, ultrasonic c-scan and microscopic inspection. *Optical Engineering*, v. 54, 10 2015. Citado 4 vezes nas páginas 7, 11, 12, and 16.

45 SEGERS, J. et al. Efficient automated extraction of local defect resonance parameters in fiber reinforced polymers using data compression and iterative amplitude thresholding. *Journal of Sound and Vibration*, v. 463, p. 114958, 2019. ISSN 0022-460X. Citado 4 vezes nas páginas 7, 9, 16, and 18.

46 MEI, H. et al. Vibration-based in-situ detection and quantification of delamination in composite plates. *Sensors*, Multidisciplinary Digital Publishing Institute, v. 19, n. 7, p. 1734, 2019. Citado 2 vezes nas páginas 7 and 16.

47 ANDLEEB, Z. et al. Multiphysics study of infrared thermography (irt) applications. *The International Journal of Multiphysics*, International Society of Multiphysics, v. 14, n. 3, p. 249–272, 2020. Citado na página 7.

48 BALAGEAS, D. et al. Thermal (ir) and other ndt techniques for improved material inspection. *Journal of nondestructive evaluation*, Springer, v. 35, n. 1, p. 18, 2016. Citado 2 vezes nas páginas 7 and 16.

49 SHANG, S.; YUN, G. J.; QIAO, P. Delamination identification of laminated composite plates using a continuum damage mechanics model and subset selection technique. IOP Publishing, v. 19, n. 5, p. 055024, apr 2010. Citado 2 vezes nas páginas 7 and 16.

50 LIU, B. et al. Experimental evaluation of pulsed thermography, lock-in thermography and vibrothermography on foreign object defect (fod) in cfrp. *Sensors*, Multidisciplinary Digital Publishing Institute, v. 16, n. 5, p. 743, 2016. Citado 3 vezes nas páginas 7, 11, and 16.

51 GHORASHI, S. A.; HONARVAR, F.; TABATABAEIPOUR, M. Automated extraction of local defect resonance using the principal component analysis in lock-in ultrasonic vibrothermography. *Infrared Physics & Technology*, Elsevier, v. 105, p. 103204, 2020. Citado 2 vezes nas páginas 7 and 8.

52 IBARRA-CASTANEDO, C. et al. Comparative study of active thermography techniques for the nondestructive evaluation of honeycomb structures. *Research in Nondestructive Evaluation*, Taylor & Francis, v. 20, n. 1, p. 1–31, 2009. Citado na página 7.

53 RANTALA, J.; WU, D.; BUSSE, G. Amplitude-modulated lock-in vibrothermography for nde of polymers and composites. *Research in Nondestructive Evaluation*, Springer, v. 7, n. 4, p. 215–228, 1996. Citado na página 7.

54 DEMY, P.; GOLINVAL, J.-C.; SIMON, D. Damage detection and local resonances model in cfrp composite material by vibrothermography. In: *ISMA2012-International Conference on Noise and Vibration Engineering*. [S.l.: s.n.], 2012. Citado 3 vezes nas páginas 7, 9, and 11.

55 BAI, G. et al. Investigation of multiple cracking in glass/epoxy 2d woven composites by vibrothermography. *Quantitative InfraRed Thermography Journal*, Taylor & Francis, v. 13, n. 1, p. 35–49, 2016. Citado na página 7.

56 SALAZAR, A. et al. Characterization of delaminations by lock-in vibrothermography. *Journal of Physics: Conference Series*, IOP Publishing, v. 214, p. 012079, mar 2010. Citado 2 vezes nas páginas 7 and 11.

57 RENSHAW, J. et al. The sources of heat generation in vibrothermography. *NDT & E International*, v. 44, n. 8, p. 736–739, 2011. ISSN 0963-8695. Citado 4 vezes nas páginas 7, 9, 11, and 16.

58 KATUNIN, A.; FIDALI, M. Self-heating of polymeric laminated composite plates under the resonant vibrations: Theoretical and experimental study. *Polymer Composites*, Wiley Online Library, v. 33, n. 1, p. 138–146, 2012. Citado 3 vezes nas páginas 7, 11, and 23.

59 KATUNIN, A.; WRONKOWICZ, A. Characterization of failure mechanisms of composite structures subjected to fatigue dominated by the self-heating effect. *Composite Structures*, Elsevier, v. 180, p. 1–8, 2017. Citado 2 vezes nas páginas 7 and 11.

60 SOLODOV, I. et al. Highly-efficient and noncontact vibro-thermography via local defect resonance. *Quantitative InfraRed Thermography Journal*, Taylor & Francis, v. 12, n. 1, p. 98–111, 2015. Citado 2 vezes nas páginas 8 and 9.

61 HETTLER, J. et al. Detection and characterization of local defect resonances arising from delaminations and flat bottom holes. *Journal of Nondestructive Evaluation*, Springer, v. 36, n. 1, p. 1–10, 2017. Citado na página 8.

62 KATUNIN, A. A concept of thermographic method for non-destructive testing of polymeric composite structures using self-heating effect. *Sensors*, v. 18, n. 1, 2018. ISSN 1424-8220. Disponível em: <https://www.mdpi.com/1424-8220/18/1/74>. Citado 5 vezes nas páginas 9, 10, 11, 16, and 23.

63 WRONKOWICZ, A.; KATUNIN, A.; WACHLA, D. Enhancement of damage identification in composite structures with self-heating based vibrothermography. *Optik*, v. 181, p. 545–554, 2019. ISSN 0030-4026. Citado 5 vezes nas páginas 9, 11, 16, 18, and 23.

64 SEGERS, J. et al. Efficient automated extraction of local defect resonance parameters in fiber reinforced polymers using data compression and iterative amplitude thresholding. *Journal of Sound and Vibration*, 09 2019. Citado 3 vezes nas páginas 9, 11, and 16.

65 MULLER, L. et al. Experimental monitoring of the self-heating properties of thermoplastic composite materials. *Procedia Engineering*, v. 213, p. 183–191, 2018. ISSN 1877-7058. 7th International Conference on Fatigue Design, fatigue of Design 2017, 29-30 November 2017, Senlis, France. Citado na página 9.

66 BAI, G. et al. Investigation of multiple cracking in glass/epoxy 2d woven composites by vibrothermography. *Quantitative InfraRed Thermography Journal*, Taylor & Francis, v. 13, n. 1, p. 35–49, 2016. Citado 2 vezes nas páginas 11 and 16.

67 MAJEWSKA, K.; MIELOSZYK, M.; OSTACHOWICZ, W. Active thermography as a tool for internal composite structure observation and evaluation. *International Journal of Structural Integrity*, Emerald Publishing Limited, 2018. Citado 2 vezes nas páginas 11 and 16.

68 CHI, X.; MAIO, D. D.; LIEVEN, N. Modal-based vibrothermography using feature extraction with application to composite materials. *Structural Health Monitoring*, v. 19, p. 147592171987241, 09 2019. Citado 2 vezes nas páginas 11 and 16.

69 KATUNIN, A. Criticality of the self-heating effect in polymers and polymer matrix composites during fatigue, and their application in non-destructive testing. *Polymers*, v. 11, n. 1, 2019. ISSN 2073-4360. Citado 2 vezes nas páginas 12 and 26.

70 POLIMENO, U. et al. A compact thermosonic inspection system for the inspection of composites. *Composites Part B: Engineering*, v. 59, p. 67–73, 2014. ISSN 1359-8368. Citado 2 vezes nas páginas 12 and 16.

71 SALAZAR, A. et al. Characterization of delaminations by lock-in vibrothermography. In: IOP PUBLISHING. *Journal of Physics: Conference Series*. [S.l.], 2010. v. 214, n. 1, p. 012079. Citado na página 14.

72 GLEITER, A. et al. Ultrasound lock-in thermography for advanced depth resolved defect selective imaging. *Insight*, v. 49, p. 272–274, 2007. Citado na página 14.

73 PIAU, J.-M. et al. Nondestructive testing of open microscopic cracks in plasma-sprayed-coatings using ultrasound excited vibrothermography. *Nondestructive Testing and Evaluation*, Taylor & Francis, v. 23, n. 2, p. 109–120, 2008. Citado na página 14.

74 IBARRA-CASTANEDO, C. et al. Chapter x active infrared thermography techniques for the nondestructive testing of materials. 05 2007. Citado na página 14.

75 ZWESCHPER, T. et al. Frequency-modulated elastic wave thermography. In: SPIE. *Thermosense XXV*. [S.l.], 2003. v. 5073, p. 386–391. Citado na página 14.

76 DEANE, S. et al. Application of ndt thermographic imaging of aerospace structures. *Infrared Physics & Technology*, v. 97, p. 456–466, 2019. ISSN 1350-4495. Citado 2 vezes nas páginas 14 and 16.

77 DENG, K. et al. Classification of barely visible impact damage in composite laminates using deep learning and pulsed thermographic inspection. *Neural Computing and Applications*, Springer, p. 1–15, 2023. Citado na página 15.

78 HILLEN, M. et al. Qualitative comparison of lock-in thermography (lit) and pulse phase thermography (ppt) in mid-wave and long-wave infrared for the inspection of paintings. *Applied Sciences*, v. 13, n. 7, 2023. ISSN 2076-3417. Citado na página 15.

79 TAO, N. et al. Analysis of step-heating thermography methods for defect depth prediction. *NDT & E International*, v. 135, p. 102800, 2023. ISSN 0963-8695. Citado na página 15.

80 WEI, J. et al. Quantitative characterization of interfacial defects in thermal barrier coatings by long pulse thermography. *Coatings*, v. 12, n. 12, 2022. ISSN 2079-6412. Citado na página 15.

81 PITARRESI, G. et al. Frequency modulated thermography-ndt of polymer composites by means of human-controlled heat modulation. In: RIZZO, P.; MILAZZO, A. (Ed.). *European Workshop on Structural Health Monitoring*. Cham: Springer International Publishing, 2023. p. 610–618. Citado na página 15.

82 ROEMER, J. et al. Data processing scheme for laser spot thermography applied for nondestructive testing of composite laminates. *Journal of Nondestructive Evaluation*, v. 42, 02 2023. Citado na página 15.

83 LIU, C. et al. Intralaminar crack detection for carbon fiber reinforced polymers based on laser-line thermography. In: *2022 8th International Conference on Mechanical Engineering and Automation Science (ICMEAS)*. [S.l.: s.n.], 2022. p. 178–184. Citado na página 15.

84 MEVISSEN, F.; MEO, M. Ultrasonically stimulated thermography for crack detection of turbine blades. *Infrared Physics & Technology*, v. 122, p. 104061, 2022. ISSN 1350-4495. Citado na página 15.

85 FIERRO, G. P. M. et al. Nonlinear ultrasonic stimulated thermography for damage assessment in isotropic fatigued structures. *Journal of Sound and Vibration*, v. 404, p. 102–115, 2017. ISSN 0022-460X. Citado na página 15.

86 WILSON, J. et al. Modelling and evaluation of eddy current stimulated thermography. *Nondestructive Testing and Evaluation*, Taylor & Francis, v. 25, n. 3, p. 205–218, 2010. Citado na página 15.

87 LEVESQUE, P.; DEOM, A.; BALAGEAS, D. Non destructive evaluation of absorbing materials using microwave stimulated infrared thermography. *Review of Progress in Quantitative Nondestructive Evaluation: Volumes 12A and 12B*, Springer, p. 649–654, 1993. Citado na página 15.

88 SAKAGAMI, T.; OGURA, K. A new flaw inspection technique based on infrared thermal images under joule effect heating. *Transactions of the Japan Society of Mechanical Engineers Series A*, v. 58, n. 555, p. 2224–2231, 1992. Citado na página 15.

89 AHMED, T. et al. Heat emitting layers for enhancing nde of composite structures. *Composites Part A: Applied Science and Manufacturing*, Elsevier, v. 39, n. 6, p. 1025–1036, 2008. Citado na página 15.

90 VILLORIA, R. G. D. et al. Multi-physics damage sensing in nano-engineered structural composites. *Nanotechnology*, IOP Publishing, v. 22, n. 18, p. 185502, 2011. Citado na página 15.

91 PINTO, F. et al. Multifunctional smart composite material for in situ ndt/shm and de-icing. *Smart Materials and Structures*, IOP Publishing, v. 21, n. 10, p. 105010, aug 2012. Citado na página 15.

92 FERNANDES, H. et al. Carbon fiber composites inspection and defect characterization using active infrared thermography: numerical simulations and experimental results. *Appl. Opt.*, OSA, v. 55, n. 34, p. D46–D53, Dec 2016. Citado na página 16.

93 ZHANG, H. et al. Comparative study of microlaser excitation thermography and microultrasonic excitation thermography on submillimeter porosity in carbon fiber reinforced polymer composites. *Optical Engineering*, v. 56, p. 041304, 04 2017. Citado na página 16.

94 ZHANG, H. et al. Enhanced infrared image processing for impacted carbon/glass fiber-reinforced composite evaluation. *Sensors*, Multidisciplinary Digital Publishing Institute, v. 18, n. 1, p. 45, 2018. Citado 2 vezes nas páginas 16 and 18.

95 VADDI, J. S.; HOLLAND, S. D.; KESSLER, M. R. Loss modulus measurement of a viscoelastic polymer at acoustic and ultrasonic frequencies using vibrothermography. *Measurement*, Elsevier, v. 168, p. 108311, 2021. Citado na página 16.

96 CHI, X.; MAIO, D. D.; LIEVEN, N. A. Modal-based vibrothermography using feature extraction with application to composite materials. *Structural Health Monitoring*, v. 19, n. 4, p. 967–986, 2020. Citado na página 18.

97 CHI, X. et al. Viability of image compression in vibrothermography. *Experimental Techniques*, Springer, v. 45, n. 3, p. 345–362, 2021. Citado na página 18.

98 ZHANG, Y. et al. Cluster analysis of acoustic emission signals and infrared thermography for defect evolution analysis of glass/epoxy composites. *Infrared Physics & Technology*, Elsevier, v. 112, p. 103581, 2021. Citado na página 18.

99 DEPARTMENT of Applied Mechanics, Faculty of Mechanical Engineering, Budapest University of Technology and Economics © 2022. 2024. Disponível em: <https://www.mm.bme.hu/~gyebro/files/ans_help_v182/ans_elem/>. Citado na página 21.

100 DANILIN, A.; SHALASHILIN, A. et al. Hysteresis modelling of mechanical systems at nonstationary vibrations. *Mathematical Problems in Engineering*, Hindawi, v. 2018, 2018. Citado na página 23.

101 KATUNIN, A.; FIDALI, M. Self-heating of polymeric laminated composite plates under the resonant vibrations: Theoretical and experimental study. *Polymer Composites*, v. 33, n. 1, p. 138–146, 2012. Citado na página 23.

102 TSCHOEGL, N. W. *The phenomenological theory of linear viscoelastic behavior: an introduction*. [S.l.]: Springer Science & Business Media, 2012. Citado na página 24.

103 MEYERS, M. A.; CHAWLA, K. K. *Mechanical behavior of materials*. [S.l.]: Cambridge university press, 2008. Citado na página 24.

104 GUPTA, A.; PANDA, S.; REDDY, R. S. Improved damping in sandwich beams through the inclusion of dispersed graphite particles within the viscoelastic core. *Composite Structures*, Elsevier, v. 247, p. 112424, 2020. Citado na página 26.

105 PUENTES, J. et al. Moduli development of epoxy adhesives during cure. *Polymer Testing*, Elsevier, v. 77, p. 105863, 2019. Citado na página 26.

106 SZMIDT, T. et al. Double-beam cantilever structure with embedded intelligent damping block: Dynamics and control. *Journal of Sound and Vibration*, Elsevier, v. 401, p. 127–138, 2017. Citado na página 26.

107 RITTEL, D. An investigation of the heat generated during cyclic loading of two glassy polymers. part i: Experimental. *Mechanics of Materials*, Elsevier, v. 32, n. 3, p. 131–147, 2000. Citado na página 26.

108 FRANCK, A.; GERMANY, T. Viscoelasticity and dynamic mechanical testing. *TA Instruments, New Castle, DE, USA AN004*, 1993. Citado na página 26.

109 HERTZBERG, R.; MANSON, J. *Fatigue of Engineering Plastics*. [S.l.]: Academic Press, 1980. ISBN 9780123435507. Citado na página 26.

6 APPENDIX

6.1 APPENDIX A - INSTRUMENTATION

- POWER AMPLIFIER

Figure 41 – Power Amplifier - 790 series

- SIGNAL ANALYZER
  Description: Signal analyser Brüel & Kjaer
  Model: PHOTON+ model
  Characterístics: 4 inputs and one output

Figure 42 – Signal analyzer

- DYNAMIC MECHANICAL ANALYSIS TEST MACHINE
- NANOINDENTATION TESTER
- PIEZOELECTRIC ACTUATOR

Figure 43 – DMA test machine

Figure 44 – Nanoindentatio tester - HIT300

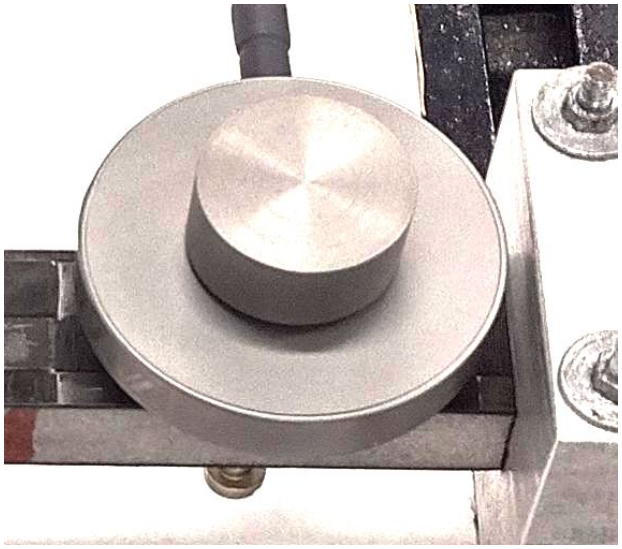

Figure 45 – Pizoeletric

6.2 APPENDIX B - SPECIMENS 2 AND 3

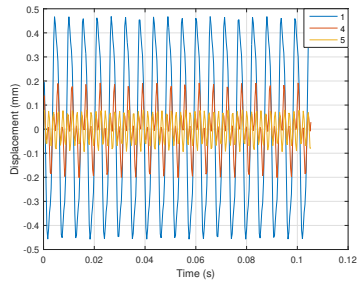

(a) 179.44 Hz

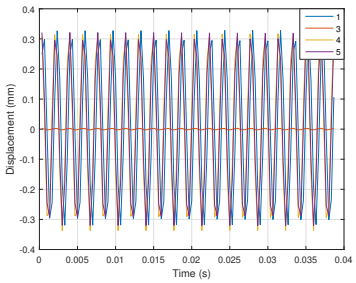

(b) 545.65 Hz

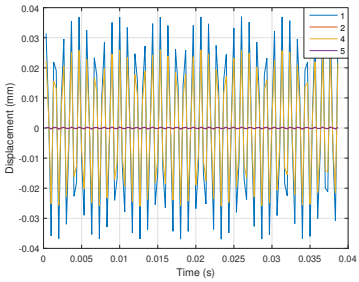

(c) 938.96 Hz

Figure 46 – Displacements reference points specimen 2

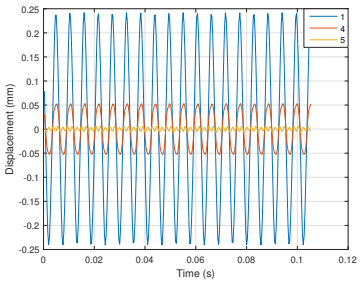

(a) 179.44 Hz

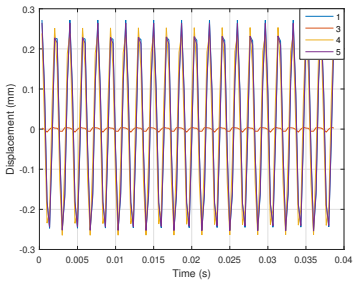

(b) 545.65 Hz

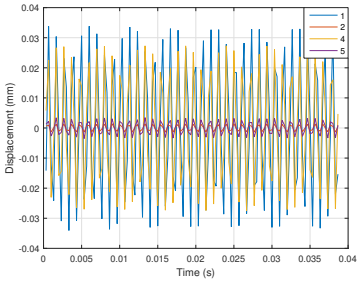

(c) 938.96 Hz

Figure 47 – Displacements reference points specimen 3

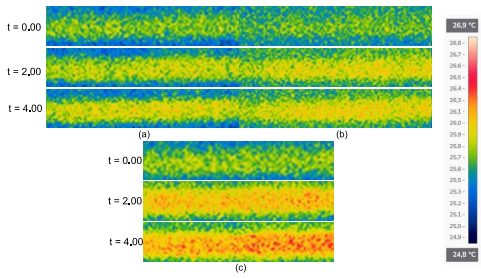

(a) 179.44 Hz

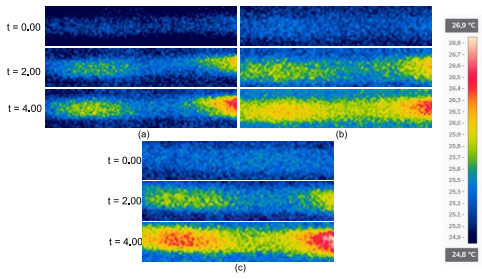

(b) 545.65 Hz

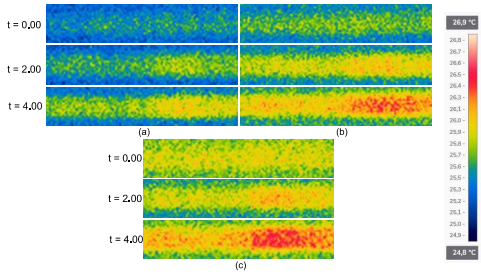

(c) 938.96 Hz

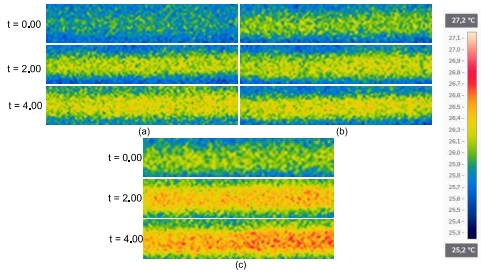

(a) 179.44 Hz

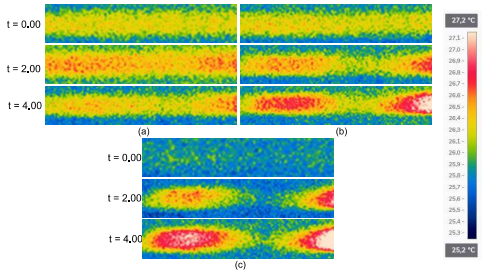

(b) 545.65 Hz

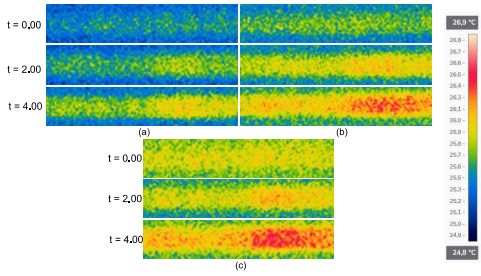

(c) 938.96 Hz